CRITICAL STING LENGTH AS DETERMINED BY THE MEASUREMENT OF PITCH-DAMPING DERIVATIVES FOR LAMINAR, TRANSITIONAL, AND TURBULENT BOUNDARY LAYERS AT MACH NUMBER 3 FOR REDUCED FREQUENCIES OF 0.0033 AND 0.0056

VON KÁRMÁN GAS DYNAMICS FACILITY
ARNOLD ENGINEERING DEVELOPMENT CENTER
AIR FORCE SYSTEMS COMMAND
ARNOLD AIR FORCE STATION, TENNESSEE 37389

July 1977

Final Report for Period July 1, 1975 — April 17, 1977

Prepared for

DIRECTORATE OF TEST ENGINEERING
DEPUTY FOR OPERATIONS
ARNOLD ENGINEERING DEVELOPMENT CENTER
AIR FORCE SYSTEMS COMMAND
ARNOLD AIR FORCE STATION, TENNESSEE 37389

NOTICES

When U. S. Government drawings specifications, or other data are used for any purpose other than a definitely related Government procurement operation, the Government thereby incurs no responsibility nor any obligation whatsoever, and the fact that the Government may have formulated, furnished, or in any way supplied the said drawings, specifications, or other data, is not to be regarded by implication or otherwise, or in any manner licensing the holder or any other person or corporation, or conveying any rights or permission to manufacture, use, or sell any patented invention that may in any way be related thereto.

Qualified users may obtain copies of this report from the Defense Documentation Center.

References to named commercial products in this report are not to be considered in any sense as an endorsement of the product by the United States Air Force or the Government.

This report has been reviewed by the Information Office (OI) and is releasable to the National Technical Information Service (NTIS). At NTIS, it will be available to the general public, including foreign nations.

APPROVAL STATEMENT

This technical report has been reviewed and is approved for publication.

FOR THE COMMANDER

Marion L. Laster

MARION L. LASTER
Director of Test Engineering
Deputy for Operations

Alan L Devereaux

ALAN L. DEVEREAUX
Colonel, USAF
Deputy for Operations

REPORT DOCUMENTATION PAGE

READ INSTRUCTIONS BEFORE COMPLETING FORM

1 REPORT NUMBER: AEDC-TR-77-66

2 GOVT ACCESSION NO.:

3 RECIPIENT'S CATALOG NUMBER:

4 TITLE (and Subtitle): CRITICAL STING LENGTH AS DETERMINED BY THE MEASUREMENT OF PITCH-DAMPING DERIVATIVES FOR LAMINAR, TRANSITIONAL, AND TURBULENT (Continued)

5 TYPE OF REPORT & PERIOD COVERED: Final Report, July 1, 1975 - April 17, 1977

6 PERFORMING ORG REPORT NUMBER:

7 AUTHOR(s): Bob L. Uselton and Fred B. Cyran, ARO, Inc.

8 CONTRACT OR GRANT NUMBER(s):

9 PERFORMING ORGANIZATION NAME AND ADDRESS: Arnold Engineering Development Center, Air Force Systems Command, Arnold Air Force Station, Tennessee 37389

10 PROGRAM ELEMENT PROJECT, TASK AREA & WORK UNIT NUMBERS: Program Element 65807F

11 CONTROLLING OFFICE NAME AND ADDRESS: Arnold Engineering Development Center (XRFIS), Arnold Air Force Station, Tennessee 37389

12 REPORT DATE: July 1977

13 NUMBER OF PAGES: 65

14 MONITORING AGENCY NAME & ADDRESS(if different from Controlling Office):

15 SECURITY CLASS. (of this report): UNCLASSIFIED

15a DECLASSIFICATION DOWNGRADING SCHEDULE: N/A

16 DISTRIBUTION STATEMENT (of this Report)

Approved for public release; distribution unlimited.

17 DISTRIBUTION STATEMENT (of the abstract entered in Block 20, if different from Report)

18 SUPPLEMENTARY NOTES

Available in DDC

19 KEY WORDS (Continue on reverse side if necessary and identify by block number)

literature surveys	Mach number
damping	interference
pitch (motion)	oscillation (forced)
boundary layer	test methods
supersonic flow	

20 ABSTRACT (Continue on reverse side if necessary and identify by block number)

A research program was initiated for the purpose of investigating some of the problem areas in regard to support interference in supersonic wind tunnels. The critical sting length at $\alpha = 0$ was determined by the measurement of pitch-damping derivatives for laminar, transitional, and turbulent boundary layers at the model base. The effect of wedge splitter plates on sting interference was also investigated. By utilizing the small amplitude forced

DD FORM 1 JAN 73 1473 EDITION OF 1 NOV 65 IS OBSOLETE

4. TITLE (Continued)

BOUNDARY LAYERS AT MACH NUMBER 3 FOR REDUCED FREQUENCIES OF 0.0033 AND 0.0056

20. ABSTRACT (Continued)

oscillation technique, data were obtained at Mach number 3 on a blunt 7-deg cone for reduced frequencies of 0.0033 and 0.0056. Model base pressure and a model surface pressure near the base were measured in addition to the pitch damping derivatives. Reynolds number, based on model base diameter, ranged from 0.3×10^6 to 4.6×10^6. The results showed that the critical sting length with respect to sting interference on pitch-damping data was two model diameters for the two reduced frequencies investigated and was independent of the type of boundary layer at the model base. In general, the addition of the wedge plates behind the model produced no effect on the damping derivatives. Decreasing the effective sting length from 3.3 to one model diameter increased the model base pressure substantially and the model surface pressure slightly. The critical sting length for minimal base pressure interference is 2.5 model diameters for this model and these test conditions.

PREFACE

The research reported herein was conducted by the Arnold Engineering Development Center (AEDC), Air Force Systems Command (AFSC), under Program Element 65807F. The results presented herein were obtained by ARO, Inc., AEDC Division (a Sverdrup Corporation Company), operating contractor for the AEDC, AFSC, Arnold Air Force Station, Tennessee. The work was done under ARO Project Numbers V32A-04A, V41A-J0A, V32A-A1A, and V41A-N9A. The authors of this report are Bob L. Uselton and Fred B. Cyran, ARO, Inc. Kenneth B. Harwood, Major, CF, is the Air Force Project Manager. The manuscript (ARO Control No. ARO-VKF-TR-77-35) was submitted for publication on May 10, 1977.

CONTENTS

ILLUSTRATIONS

Figure

Figure | Page

TABLES

1.0 INTRODUCTION

Many questions have been asked concerning model support interference effects on data obtained in supersonic wind tunnels. In general, answers have not been found. The aerodynamicist, who must rely on theoretical and experimental information for prediction of full-scale flight behavior, has in the last few years become more concerned about support interference. As accuracy requirements imposed on wind tunnel data become more stringent, the evaluation of model support interference effects becomes critical.

A research program was initiated at the Arnold Engineering Development Center (AEDC), von Kármán Gas Dynamics Facility (VKF), for the purpose of improving the understanding of some of the problems associated with support interference at supersonic Mach numbers. The majority of the work will be directed toward sting interference effects on dynamic stability derivatives. However, these results are directly applicable for estimating the onset of sting interference effects on static-stability date. This report documents the work that was completed in 1976.

The objectives of the 1976 effort were (1) to conduct a literature survey, (2) to define critical sting lengths for two reduced frequencies as determined by the measurement of pitch-damping derivatives for laminar, transitional, and turbulent boundary layers at the model base, (3) to investigate the effects on pitch-damping derivatives of wedge plates located behind the model, and (4) to investigate the surface pressure variation near the model shoulder as a function of model oscillation for interfering and non-interfering stings. Wind tunnel tests were conducted at Mach number 3 on a blunted (r_n/r_b = 0.15), 7-deg half-angle cone at reduced frequencies ($\omega d/2V_\infty$) of 0.0033 and 0.0056. Reynolds number, based on model base diameter, ranged from 0.3×10^6 to 4.6×10^6, and angle of attack varied from 0 to 8 deg. The small amplitude ($\theta = \pm 1$ deg) forced oscillation technique was utilized. The magnitude and range of the reduced frequency parameter were selected to be representative of typical wind tunnel apparatus capabilities and flight values.

2.0 STATUS OF SUPPORT INTERFERENCE

Many wind tunnel test programs have been conducted in the past for the purpose of evaluating support effects. The majority of these programs have used base pressure as the interference indicator. For

example, Whitfield (Ref. 1) points out that base pressure can serve as the first indicator of support interference. Whitfield (Ref. 1) and Pick (Ref. 2) state that the separated flow about the rear of the body depends on several variables including the geometry of the body and support, location of transition, Reynolds number, and Mach number. This appears to be very true when the available literature on support interference is reviewed. One finds that critical sting length and diameter vary widely, and the literature almost seems to indicate that support interference should be analyzed for each individual experimental program. A question which also comes to mind is whether base pressure is the correct interference indicator for all types of testing (static force, pressure, dynamic stability, etc.). Obviously, base drag is significantly affected by support interference, but what about forebody drag, static moment, lift, center of pressure, and damping derivatives?

In the discussion of the literature, base pressure will be the parameter used as the base flow interference indicator unless noted otherwise. Also unless noted, reference to base pressure will actually mean base pressure ratio, i.e., base pressure divided by free-stream static pressure. Critical sting length is generally defined as the shortest sting length which does not change the constant base pressure level obtained by longer stings. The effective sting length (ℓ_s) is defined as the distance from the model base to the first large increase of sting diameter (generally a conical taper to a larger diameter). An increased diameter is usually required at some station downstream of the model base, and such a change in sting diameter will be referred to as a flare. The effective sting diameter (d_s) is defined as the sting diameter at the model base. The sting diameter causing no interference, i.e., no effect on base pressure, is not defined since the literature shows that constant base pressure does not necessarily indicate that no interference exists. These sting dimensions are clarified later in Section 3.3. Critical sting diameter is often defined in older literature as the largest sting diameter which does not change the constant base pressure level obtained by smaller diameter stings. However, experience has shown that any finite sting diameter may impose an interference effect on base pressure, so that the concept of a critical sting diameter is not employed herein.

Whitfield (Ref. 1) reported on wind tunnel tests at Mach numbers 3 and 4 on ogive cylinders (with and without boattail). Typical variations of base pressure and critical sting length with Reynolds number are presented in Ref. 1 and are reproduced in Sketch A. From Sketch A, it is evident that if transition occurs in the wake, then base pressure

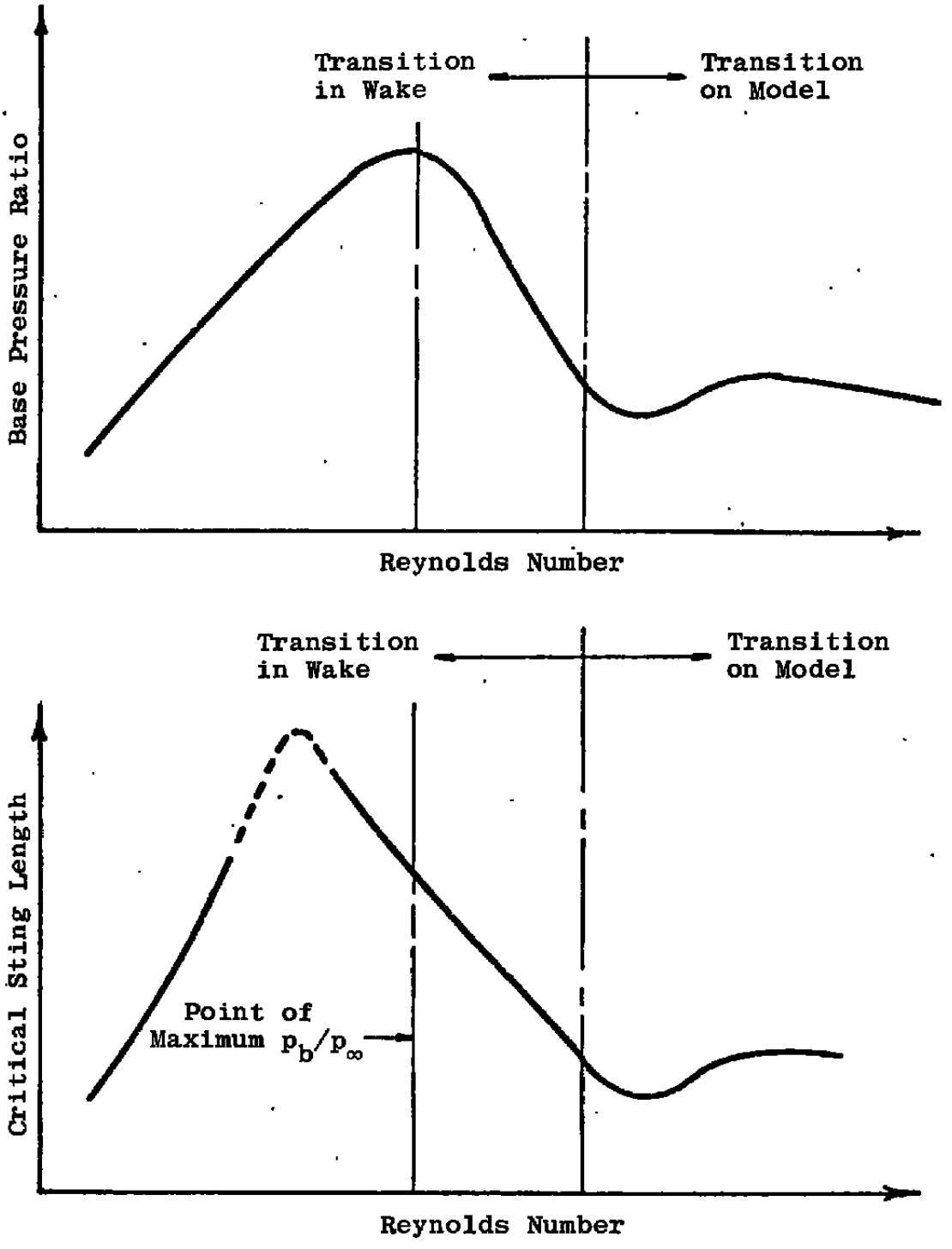

Sketch A. Typical variation of base pressure ratio and critical sting lengths with Reynolds number.

and critical sting length change rapidly with change in Reynolds number. If transition is on the model, then base pressure and critical sting length change very little with change in Reynolds number. Whitfield's results showed base pressure and critical sting length to be strong functions of transition location and length Reynolds number. Critical sting lengths of 1 to 5 model diameters were obtained depending on length Reynolds number and configuration. Forebody axial force of the boattailed models at $M_\infty = 4$ was found to be dependent on sting length, while the forebody axial force of the straight-tailed models was independent of sting length. Only after the flow was completely attached to the boattailed afterbody was the forebody axial force unaffected by sting length. Whitfield also compared critical sting length for boattailed models as determined by the forebody axial-force measurements and by the base-pressure measurements and found the agreement to be good. According to Crocco and Lee's theory (Ref. 3), disturbances downstream of the wake critical point or throat are unable to affect the flow upstream. However, Whitfield concluded that the critical point of the undisturbed wake did not represent the limit of approach of the sting flare to the model base without interference and that the sting flare should be positioned at least 1 to 1.5 base diameters downstream of the critical point. Whitfield believed that the downstream influences propagate upstream to the wake region through the layer of low energy flow surrounding the sting. Kavanau (Ref. 4) tested a cone-cylinder model at Mach number 2.84 in flow of low unit Reynolds number. Like Whitfield, he found critical sting length to be a strong function of Reynolds number with values as high as 10.5 model diameters at a low length Reynolds number of 0.05×10^6. Perkins (Ref. 5) studied the effects of support interference on ogive-cylinders with and without boattail at Mach number 1.5. His conclusions concerning support effects on base- and fore-drag of straight- and boattail-configurations with either laminar or turbulent boundary layer were essentially the same as Whitfield's. Perkins concluded that the critical sting length at $M_\infty = 1.5$ for a zero boattail configuration and either laminar or turbulent boundary layer was 5.2 model diameters for a $d_s/d = 0.3$. However, the base drag was found to depend on the support diameter (for $0.22 \leq d_s/d \leq 1$). For a boattail configuration, the critical sting length and diameter was found to be 1.7 and 0.4 model diameters, respectively. Since a boattail configuration is generally considered to be very sensitive to support interference, then one would have thought that the required critical sting length would be at least equal to that of the zero boattail configuration. Reller and Hamaker (Ref. 6) studied support effects on the base pressure of an ogive-cylinder (zero boattail) at Mach numbers 2.7 through 5. Their results showed the critical sting length to be two

model diameters at M_∞ = 2.7, 3.5, and 4 for laminar and turbulent boundary layers. At M_∞ = 5, the critical sting length was six model diameters for a laminar boundary layer and four model diameters for a turbulent boundary layer.

Sivier and Bogdonoff (Ref. 7) investigated support effects on base pressure of an ogive-cylinder model at M_∞ = 2.97 with turbulent boundary layer over the base of the model. The model was supported by a wing mounted well forward on the nose, and dummy stings were inserted into the model base to simulate different sting configurations. Sivier and Bogdonoff found that, for d_s/d = 0.375, base pressure was insensitive to Reynolds number, and the level did not change when the effective sting length was increased from 2.5 to 6 model diameters. They also found that base pressure decreased with increasing sting diameter and was Reynolds number dependent. Chapman (Ref. 8) states that this decrease in base pressure with increase in sting diameter can be explained by an interpretation of an inviscid flow. Sivier and Bogdonoff's comparison of base pressure from a d_s/d = 0.1 sting to the free base value showed the free-base value to be about 7 percent higher. However, these results could be misleading since Reichenau (Ref. 9) concluded that strut supports had little effect on the base pressure of an ogive cylinder at subsonic Mach numbers but induced significant base interference at low supersonic Mach numbers ($M_\infty \leq 1.4$). Chapman (Ref. 8) tested cone and ogive-cylinders (zero boattail) at Mach numbers 2 and 2.9. His results showed the critical sting length to be three model diameters at M_∞ = 2 for laminar or turbulent boundary layer and at M_∞ = 2.9 for turbulent boundary layer only. Reese and Wehrend (Ref. 10) investigated sting effects on the base pressure of a blunted cone-cylinder-flare-configuration at Mach numbers of 0.65 to 2.20. They found the critical sting length to be greater than 4.8 model diameters at subsonic and transonic speeds and less than 2.5 at supersonic speeds. Lee and Summers (Ref. 11) reported on sting support effects on ogive-cylinders with and without boattailing at Mach numbers 0.6 through 1.4. In general, the maximum interference effects occurred at Mach number 0.95 and were substantially smaller at M_∞ = 1.4. Lee and and Summers found the critical sting lengths (boattail model) as determined by measurements of base drag to be approximately 1 model diameter greater than those determined by the fore drag measurements.

One normally would prefer to compare free-flight data from wind tunnels or ballistic ranges with support data from wind tunnels for assessment of support interference effects. However, only a minimum of these comparisons has been made as can be seen by a review of the

literature. (Note that free-flight base pressure on aeroballistic range models usually must be determined by subtracting calculated forebody drag from measured total drag. Thus, large uncertainties may arise, particularly an α 0.) Pick (Ref. 2) presents a comparison of free-flight and sting-supported (ℓ_s/d = 11, d_s/d = 0.33) base pressure cone data at Mach numbers 6.3 and 9.9. At M_∞ = 6.3, the free-flight and sting-supported base pressures agreed at the lower angles of attack ($\alpha < 15$ deg), while for the higher angles of attack ($15 < \alpha \leq 40$ deg) the free-flight data were higher than the sting-supported data. At M_∞ = 9.9, the free-flight base pressure data were always higher than the sting-supported model base pressure by as much as 120 percent at α = 0. However, Cassanto (Ref. 12) compared free-flight and sting-supported base pressure on sharp and blunted 10-deg cones at M_∞ = 4, and found that the free-flight data (laminar boundary layer) was approximately 25 percent lower than the sting-supported data (laminar also). Cassanto states that this is the expected trend since support interference usually tends to raise the base pressure. In order to obtain turbulent flow on the free-flight models, grit was used, and excellent agreement with the turbulent sting data (without grit) was found. Cassanto also noted no radial base pressure gradient in the sting-supported data. Kavanau (Ref. 4) and Reller (Ref. 6) also found essentially no effects of base pressure orifice location; however, in Ref. 13, Cassanto reports that full-scale flight base pressures from a 10-deg sharp flat base cone at M_∞ = 20 showed radial gradients which decreased monotonically from the centerline value. Jaffe (Ref. 14) reported on free-flight and sting-supported drag data at Mach numbers 0.7 through 1.2. The test configurations were a sharp 10-deg cone, a sphere, a 60-deg blunt cone, and a blunt cylindrical configuration with tail fins. Jaffe concluded that the 60-deg cone and sphere were insensitive to the presence of stings ($\ell_s/d \approx 11$, d_s/d = 0.373 and 0.5). Comparative data for the 10-deg cone showed the sting effect to be appreciable for a d_s/d = 0.67 sting and negligible for a d_s/d = 0.37 sting. The 10-deg cone free-flight data agreed well with the d_s/d = 0.37 sting data. The free-flight drag data for the cylindrical configuration was 15 percent higher than that from the sting-supported model. Jaffe's data also showed that the fore drag for the 10-deg cone and the blunt cylindrical configuration was influenced by the presence of the sting.

In the review of the literature, it is evident that little work has been done in the area of support effects on normal-force and pitching-moment coefficients, on analytical predictions of support interference, and on dynamic stability measurements. Vlajinac and co-authors (Ref. 15) used a magnetic suspension system in conjunction with a dummy

sting ($d_s/d \approx 0.25$, $\ell_s/d \approx 4.7$) to investigate support effects at $M_\infty = 0.28$ on a 6-deg blunted cone with a bulbous base. Their results showed that the dummy sting produced considerable effects on the lift and drag coefficients. The presence of the dummy sting increased model stability so that data could be obtained at and near zero angle of attack, whereas, without the sting, it had been impossible to obtain data near $\alpha = 0$. Adcock (Ref. 16) investigated the effect of different sting offsets relative to the model base on the static coefficients of a blunt 6-deg cone with a bulbous base. His results showed significant sting effects on the static data and on model surface pressures in the base region for Mach numbers 0.26 and 0.90. Fuller and Langhans (Ref. 17), for Mach numbers 1.5 to 2.86 and ogive cylinders with and without boattail with turbulent flow, concluded that there was little effect of sting diameter ($d_s/d = 0.25$, 0.50, and 0.75, $\ell_s/d \approx 3.3$) on the static data.

The present literature review revealed records of only three attempts at determining support effects by analytical means. Tunnell (Ref. 18) presented an analysis which estimated for subsonic speeds the interference to model base pressure resulting from the presence of a conical afterbody on the sting. However, the method predicts only the base pressure trend not the absolute level. J. H. van der Zwaan[1] used the NLR panel method to predict model support interference on the lift and pitching moment characteristics of an airplane configuration at $M_\infty = 0.5$. Comparison with experimental data was fairly good. Ericsson and Reding (Ref. 19) proposed an analytical means for evaluating sting interference effects on the dynamic stability measurements of bulbous-based model configurations. The analysis relates the static and dynamic effects of separation through quasi-steady theory.

In regard to support interference effects on dynamic stability measurements, Wehrend (Ref. 20) tested a blunt 12.5-deg cone with and without a rounded base at Mach numbers 0.65, 1.0, and 1.6. His results, except for one case, showed the pitch-damping derivatives to be essentially insensitive to changes in sting length ($\ell_s/d = 0$, 1.85, and 3.7) and sting diameter ($d_s/d = 0.31$, 0.39, and 0.47). The exception was the rounded base configuration at $M_\infty = 0.65$ where both length and diameter effects were present. Uselton (Ref. 21) investigated sting support effects on a 10-deg cone at Mach numbers 2.5, 3, and 4. The critical sting length, as determined by base pressure measurements

[1] Private communication with J. H. van der Zwaan, National Aerospace Laboratory, NLR, Nederland.

with $d_s/d = 0.4$, was shown to be between 1.5 and 2.25 model diameters at $M_\infty = 2.5$ to 3 for a Reynolds number range, based on model diameter, of 0.3×10^6 to 3.6×10^6. At $M_\infty = 4$ for $Re_d \approx 1.0 \times 10^6$ to 1.9×10^6, the critical sting length was between 0.75 and 1.5 model diameters. At the lower laminar Reynolds numbers, a sting length of 3 model diameters was possibly not sufficient. Base pressure as a function of sting diameter ($0.4 \leq d_s/d \leq 0.8$) ($\ell_s/d = 3$) at $M_\infty = 2.5$ and 3 showed opposite trends depending on Reynolds number. For $Re_d \approx 0.4 \times 10^6$, base pressure increased with increasing sting diameter, and for $Re_d \approx 2.1 \times 10^6$, it decreased with increasing sting diameter. It appeared that, for both cases, the curves would come together (same base pressure) at $d_s/d = 0.2$. Uselton and co-authors (Ref. 22) found that for a 7-deg half-angle flat-base cone at $M_\infty = 3$, $\alpha = 0$, the magnitude of the sting interference effect on the damping derivatives was dependent on frequency. Their results also showed no sting interference effect on the pitching-moment coefficient. Uselton and Wallace (Ref. 23) investigated sting support effects on Viking configurations at Mach numbers from 1.6 through 3. Comparisons of the model wake geometries of the sting-supported models were made with free-flight wake geometries, and significant differences were found. These results are also documented in Ref. 24.

Several investigators have conducted tests with a splitter plate or wedge plate installed behind the model. Sallet (Ref. 25) showed that vortex shedding may be prevented by the installation of a splitter plate behind a circular cylinder, and therefore the fluctuating Karman forces may not occur. Roshko (Refs. 26 and 27) also discussed effects of plates behind circular cylinders. Baughman and Jack (Ref. 28) studied the effects of a splitter plate on and behind a cone-cylinder at $M_\infty = 3.1$. The results showed that the splitter plate effects on body and base pressures were generally small. Clay and Walchner (Ref. 29) presented data at $M_\infty = 14$ which showed that the addition of a splitter plate to the support strut behind the sting smoothed and reduced the base pressure significantly. Wehrend (Ref. 20) also added wedge plates to one sting configuration ($\ell_s/d = 3.7$, $d_s/d = 0.31$). They produced essentially no effects on the damping derivatives with the exception of a rounded-base configuration at $M_\infty = 0.65$ where the instability was decreased. References 30 through 34 are additional references which one may find of use in regard to support effects.

For convenient access, the pertinent factors from the references discussed are shown in the following summary.

Summary of Available References

References	M_∞	Reynolds Number	Boundary Layer	Model	Model Support	ℓ_s/d	d_s/d	Measurements	Findings
Whitfield, Ref. 1	3.4	$Re_\ell = 0.4 \times 10^6$ to 10×10^6	Laminar, Transitional, Turbulent	Ogive Cylinders with and without Boattails	Sting	1 to 5.75	0.3, 0.5	p_b, Drag	1. p_b and ℓ_{cr} dependent on transition location and length Reynolds number. 2. ℓ_{cr}/d = 1 to 5. 3. ℓ_{cr} determined by the measurements of fore drag and base drag were approximately equal.
Pick, Ref. 2	6.3, 9.9	$Re_\ell = 0.5 \times 10^6$	---	9 and 10 deg Cones	Sting, and Free Flight	11.0	0.33	p_b	1. Severe differences between free-flight and sting-supported base pressures.
Crocco, Ref. 3	---	---	---	---	---	---	---	---	1. Theoretical prediction of base pressure.
Kavanau, Ref. 4	2.84	$Re_\ell = 0.05 \times 10^6$ to 0.4×10^6	Laminar	Cone-Cylinder	Sting	0.5 to 10.5	0.18, 0.23	p_b	1. ℓ_{cr}/d = 3 to 10.5 depending on Re_ℓ. 2. No effect of base pressure orifice location.
Perkins, Ref. 5	1.5	$Re_\ell = 0.6 \times 10^6$ to 5×10^6	Laminar, Turbulent	Ogive Cylinders with and without Boattails	Sting, Strut	0.7 to 7.2	0.25 to 1.0	p_b, Drag	1. ℓ_{cr}/d = 5.2 for zero boattail configuration with laminar or turbulent flow. 2. ℓ_{cr}/d = 1.7 for boattail configurations with laminar or turbulent boundary layer. 3. For zero boattail configuration C_A was not affected by the presence of a rear support. 4. For a boattail configuration with laminar boundary layer. C_A was affected by the presence of a rear support.
Reller, Ref. 6	2.7 to 5	$Re_\ell = 0.6 \times 10^6$ to 8.8×10^6	Laminar, Turbulent	Ogive Cylinders	Sting	2 to 8	0.25 to 0.75	p_b	1. ℓ_{cr}/d = 2 for M_∞ = 2.7, 3.5 and 4 for laminar and turbulent boundary layer. 2. At M_∞ = 5, ℓ_{cr}/d = 6 and 4 for laminar and turbulent boundary layers, respectively. 3. Essentially no effect of base pressure orifice location.
Sevier, Ref. 7	2.97	$Re_\ell = 10 \times 10^6$ to 40×10^6	Turbulent	Ogive Cylinders	Strut and Dummy Stings	2.5 to 6	0.06 to 0.6	p_b	1. p_b decreased with increasing d_s/d and was Re_ℓ dependent. 2. For d_s/d = 0.375, p_b was insensitive to Re_ℓ. 3. Decreasing ℓ_s/d from 6 to 2.5 had no effect on p_b.

Summary of Available References
Continued

References	M_∞	Reynolds Number	Boundary Layer	Model	Model Support	ℓ_s/d	d_s/d	Measurements	Findings
Chapman, Ref. 8	2, 2.9	$Re_\ell = 4 \times 10^6$ to 7.5×10^6	Laminar, Turbulent	Cone-and Ogive-Cylinders	Sting	1.2 to 4.4	0 to 1	p_b	1. $\ell_{cr}/d = 3$ at $M_\infty = 2$ for laminar and turbulent boundary layer. 2. $\ell_{cr}/d = 3$ at $M_\infty = 2.9$ for turbulent boundary layer. 3. p_b generally decreased with increasing d_s/d.
Reichenau, Ref. 9	0.7 to 1.4	$Re_\ell = 2.7 \times 10^6$ to 3.3×10^6	—	Ogive Cylinder	Strut, Sting	2.4 to 8.4	0.5	p_b, p_s	1. Strut configurations had little effect on p_b at subsonic M_∞ but induced significant base interference at low supersonic M_∞.
Reese, Ref. 10	0.65 to 2.2	$Re_d = 0.5 \times 10^6$ to 1.1×10^6	—	Blunt-Cylinder-Flare	Sting	2.5 to 4.8	0.23 to 0.59	p_b	1. $\ell_{cr}/d > 4.8$ for subsonic M_∞. 2. $\ell_{cr}/d < 2.5$ for supersonic M_∞.
Lee, Ref. 11	0.6 to 1.4	$Re_\ell = 8 \times 10^6$	—	Ogive Cylinder with and without Boattail	Strut, Sting	0 to 8.5	0.25 to 0.75	p_b, Drag	1. Cylindrical model: $\ell_{cr}/d = 4.5$ at $M_\infty = 0.8$, $\ell_{cr}/d = 5.5$ at $M_\infty = 0.95$, $\ell_{cr}/d = 2.6$ at $M_\infty = 1.4$ all for $d_s/d = 0.5$ and based on p_b. 2. Boattail model: $\ell_{cr}/d = 5.1$ at $M_\infty = 0.8$, $\ell_{cr}/d = 6.1$ at $M_\infty = 0.95$, $\ell_{cr}/d = 4.3$ at $M_\infty = 1.4$ all for $d_s/d = 0.43$ and based on p_b. 3. Critical sting lengths for the boattail model determined by measurements of base drag were approximately 1 model diameter greater than those determined by fore drag.
Cassanto, Ref. 12	4	$Re_\ell \approx 0.4 \times 10^6$ to 10×10^6	Laminar, Transitional, Turbulent	10-deg Cone	Free Flight, Sting	—	0.25	p_b	1. For laminar boundary layer, $(p_b)_{free} = 0.75\ (p_b)_{sting}$. 2. For turbulent boundary layer, $(p_b)_{free} = (p_b)_{sting}$. 3. Found no radial gradients in sting base pressure data.
Cassanto, Ref. 13	≈ 20	$Re_\ell = 0.5_6 \times 10^6$ to 7×10^6	Laminar,	10-deg Cone	Flight Data	—	—	p_b	1. Flight base pressures showed radial gradients which decreased monotonically from the centerline value.

Summary of Available References
Continued

References	M_∞	Reynolds Number	Boundary Layer	Model	Model Support	ℓ_s/d	d_s/d	Measurements	Findings
Jaffe, Ref. 14	0.7 to 1.2	Re/ft = 1.5 x 10^6 to 3.5 x 10^6	Turbulent	10-deg Cone, Sphere, 60-deg Cone, Blunt Cylindrical Configuration	Free Flight, Sting	7 to 11.6	0.37 to 1.0	P_b, Drag	1. 60-deg cone and sphere were insensitive to the presence of the sting. 2. For 10-deg cone, sting effect was appreciable for d_s/d = 0.67 and negligible for d_s/d = 0.37. Comparison of free flight data with d_s/d = 0.37 data was good. 3. The fore drag for the 10-deg cone and blunt cylindrical configuration was influenced by the presence of the sting. 4. The free-flight drag data for the blunt configuration was 15 percent higher than the sting data.
Vlajinac, Ref. 15	0.28	Re_d = 0.12 x 10^6	Turbulent	6-deg Cone with Bulbous Base	Magnetic Suspension with Dummy Sting	4.7	0.25	Lift, Drag	1. The presence of the sting (d_s/d = 0.25, ℓ_s/d = 4.7) produced considerable effects on the lift and drag. 2. The sting increased model stability at and near α = 0.
Adcock, Ref. 16	0.26 and 0.9	Re_d = 1.2 x 10^6	Turbulent	6-deg Cone with Bulbous Base	Sting	—	—	Static Coefficients, Surface Pressure	1. Offset stings relative to the model base produced significant effects on the static data and the model surface pressures in the base region.
Fuller, Ref. 17	1.5 to 2.86	Re_d = 0.75 x 10^6	Turbulent	Ogive-Cylinders with and without Boattails	Strut with Dummy Stings	3.3	0.25, 0.5, 0.75	Static Coefficients	1. Variation of d_s/d from 0 to 0.75 showed little effect on the static data.
Tunnell, Ref. 18	0.6 to 1.3	—	Turbulent	Winged Vehicle	Sting	0.5 to 4.6	0.85, 0.93	P_b, Drag	1. Theoretical prediction of base pressure resulting from conical flare on sting. 2. Sting length effects were a maximum in the subsonic-transonic region.
van der Zwaan	0.5	—	—	Winged Vehicle	Strut, Sting	—	—	Lift, C_m	1. Theoretical predictions of support interference on lift and pitching moment agreed well with experimental data.
Ericsson, Ref. 19	—	—	—	Blunt and Slender Cones with Rounded Bases	—	—	—	—	1. Proposed on analytical means for evaluating sting interference effects in dynamic stability measurements on bulbous-base configurations. 2. Discussed effects of separated flow about bulbous-base configurations.

Summary of Available References
Continued

References	M_∞	Reynolds Number	Boundary Layer	Model	Model Support	ℓ_s/d	d_s/d	Measurements	Findings
Wehrend, Ref. 20	0.65, 1.0 1.6	$Re_d = 0.68 \times 10^6$ to 1.54×10^6	—	12.5-deg Blunt Cone with and without Rounded Base	Sting	0, 1.85, 3.7	0.31 to 0.47	$C_{m_q} + C_{m_{\dot\alpha}}$	1. Variation of ℓ_s/d = 0 to 3.7 and d_s/d = 0.31 to 0.47 affected $C_{m_q} + C_{m_{\dot\alpha}}$ only at M_∞ = 0.65 for the rounded-base configuration. 2. Results should be used with caution since interference hardware was attached to the sting. 3. The addition of a plate to the sting (ℓ_s/d = 3.7) decreased model instability at M_∞ = 0.65 (rounded base), but had essentially no effect of M_∞ = 1 and 1.6.
Uselton, Ref. 21	2.5, 3.4	$Re_d = 0.45 \times 10^6$ to 10.2×10^6	Laminar, Transitional, Turbulent	10-deg Cone	Sting	0.75 to 3	0.2 to 0.8	p_b, $C_{m_q} + C_{m_{\dot\alpha}}$, C_{m_α}	1. ℓ_{cr}/d, as determined by p_b, for d_s/d = 0.4, was between 1.5 and 2.25 for M_∞ = 2.5 and 3. At M_∞ = 4, ℓ_{cr}/d was between 0.75 and 1.5 for turbulent boundary layer. 2. Interference damping results should be used with caution since interference hardware was attached to sting.
Uselton, Ref. 22	3	$Re_d = 3.2 \times 10^6$	Turbulent	7-deg Cone	Sting	1 to 5	0.22	$C_{m_q} + C_{m_{\dot\alpha}}$, C_m	1. Magnitude of the sting interference effect was frequency dependent. 2. Decreasing ℓ_s/d from 3.5 to 1 produced no effects on C_m.
Uselton, Ref. 23 Steinberg, Ref. 24	1.6 to 3	$Re_d = 0.25 \times 10^6$ to 1.49×10^6	—	70-deg Cone	Sting, Free Flight	1.5 to 3.5	0.18 to 0.53	$C_{m_q} + C_{m_{\dot\alpha}}$ Wake Geometry	1. Wake geometries of sting-supported models showed significant differences as compared to free-flight wake geometries. 2. Interference damping results should be used with caution since interference hardware was attached to sting.
Sallet, Ref. 25 Roshko, Refs. 26 and 27	—	—	—	—	—	—	—	—	1. Discussion of effects of splitter or wedge plates behind circular cylinders.
Baughman, Ref. 28	3.1	$Re_\ell = 2 \times 10^6$ to 14×10^6	—	Cone Cylinder	Sting	4	0.5	p, p_b	1. Splitter plate effects on body and base pressures were generally small.

Summary of Available References
Concluded

References	M_∞	Reynolds Number	Boundary Layer	Model	Model Support	ℓ_s/d	d_s/d	Measurements	Findings
Clay, Ref. 29	14	$Re_\ell \approx 0.6 \times 10^6$	—	Blunt 5.6-deg Cone	Sting	1.2, 4.2	—	P_b	1. The addition of a splitter plate to the support strut behind the sting smoothed and reduced P_b significantly.
Love, Ref. 30	Transonic, Supersonic	—	—	—	—	—	—	—	1. Summary of support interference problems at transonic and supersonic speeds.
Sieling, Ref. 31	3.88	$Re_d = 3.9 \times 10^6$	Turbulent	Nose-Cylinder	Sting	0 to 4	0 to 0.5	P_b	1. $d_s/d > 0.15$ influenced base pressure by more than 4 percent. 2. The base pressure was unaffected by sting length for $\ell_s/d > 1.3$.
Peckham, Ref. 32	6.8	—	Laminar, Transitional	Delta Wing, Cone	Sting	3.1 to 6.3	0.3 to 0.8	Schlieren Photographs	1. Results showed that short sting lengths have less support interference if transition occurs upstream of the model base.
Trescot, Ref. 33	1.5 to 4	$Re_d = 0.16 \times 10^6$ to 0.41×10^6	—	70-deg Cone	Sting	5.8	0.12 to 0.5	Static Coefficients, P_b	1. At $M_\infty = 1.5$ and 2 an increase in d_s decreased P_b and increased the axial-force coefficient. No appreciable effect was found at $M_\infty = 3$ and 4.
Hart, Ref. 34	0.7 to 1.3	$Re_\ell = 15 \times 10^6$ to 45×10^6	—	Ogive-Cylinder with and without Fins	Flight Tests with Dummy Stings	2.4	0.6	P_b	1. The sting reduced base suction by about 40 percent at subsonic-transonic speeds, but had no measurable effect for $M_\infty > 1.15$.

The author also has compiled a chart of suggested critical sting lengths for various configurations for the range of Mach numbers from subsonic to hypersonic. The chart is based on data in the literature, and it is the intention that it be used as a guide in the selection of support stings and in evaluating existing data for sting length effects. The chart readily points out the scarcity of sting criteria and also how future interference tests at AEDC will be helpful in filling data voids in the chart. Critical sting diameter is not listed because the base pressure trends with sting diameter sometimes do not indicate a critical diameter (constant base pressure does not necessarily indicate critical sting diameter, see Ref. 7). However, the author believes that, if $d_s/d \leq 0.3$, then the diameter intereference effect, if existent, is a minimum. The sting criteria and notes are listed below.

Suggested Sting Criteria[a]

Models	Mach Regime	Mach Number	Measurements	Boundary Layer[b]	Critical Sting Length, $\approx \ell_{cr}/d$
Nose-Cylinder without Boattail	Subsonic	0.6 to 0.9	P_b, C_A	Unknown	6
		—	C_N, C_m	—	No Data
		—	$C_{m_q} + C_{m_{\dot{\alpha}}}$	—	No Data
	Transonic	0.95 to 1.2	P_b, C_A	Unknown	6
		—	C_N, C_m	—	No Data
		—	$C_{m_q} + C_{m_{\dot{\alpha}}}$	—	No Data
	Supersonic	1.5 to 5	P_b, C_A	Laminar	3 to 10[c]
		1.5 to 4	P_b, C_A	Turbulent	2 to 3
		5	P_b, C_A	Turbulent	4
		—	C_N, C_m	Laminar	No Data
		1.5 to 3	C_N, C_m	Turbulent	$\ell_{cr}/d \leq 3.3$[d]
		—	$C_{m_q} + C_{m_{\dot{\alpha}}}$	—	No Data
	Hypersonic	—	P_b, C_A	—	No Data
		—	C_N, C_m	—	No Data
		—	$C_{m_q} + C_{m_{\dot{\alpha}}}$	—	No Data
Nose-Cylinder with Boattail	Subsonic	0.6 to 0.9	P_b, C_A	Unknown	6
		—	C_N, C_m	—	No Data
		—	$C_{m_q} + C_{m_{\dot{\alpha}}}$	—	No Data

Suggested Sting Criteria[a] Continued

Models	Mach Regime	Mach Number	Measurements	Boundary Layer[b]	Critical Sting Length, $\approx \ell_{cr}/d$
Nose-Cylinder with Boattail	Transonic	0.95 to 1.2	p_b, C_A	Unknown	6
		—	C_N, C_m	—	No Data
		—	$C_{m_q} + C_{m_{\dot{\alpha}}}$	—	No Data
	Supersonic	1.5 to 5	p_b, C_A	Laminar	5 to 10[c]
		1.5 to 4	p_b, C_A	Turbulent	$\ell_{cr}/d \leq 3$[d]
		—	C_N, C_m	Laminar	No Data
		1.5 to 3	C_N, C_m	Turbulent	$\ell_{cr}/d \leq 3.3$[d]
		—	$C_{m_q} + C_{m_{\dot{\alpha}}}$	—	No Data
	Hypersonic	—	p_b, C_A	—	
		—	C_N, C_m	—	
		—	$C_{m_q} + C_{m_{\dot{\alpha}}}$	—	
Slender-Flat-Base Cones	Subsonic	—	p_b, C_A	—	
		—	C_N, C_m	—	
		—	$C_{m_q} + C_{m_{\dot{\alpha}}}$	—	
	Transonic	—	p_b, C_A	—	
		—	C_N, C_m	—	
		—	$C_{m_q} + C_{m_{\dot{\alpha}}}$	—	
	Supersonic[e]	2 to 3	p_b, C_A	Laminar	2.5
		2 to 3	p_b, C_A	Turbulent	2.5
		4	p_b, C_A	Laminar	$\ell_{cr}/d > 3$[f]
		4	p_b, C_A	Turbulent	1.5
		3	C_N, C_m	Laminar	2
		3	C_N, C_m	Turbulent	2
		3	$C_{m_q} + C_{m_{\dot{\alpha}}}$	Laminar	2[g]
		3		Transitional	2[g]
		3		Turbulent	2[g]
	Hypersonic[e]	14	p_b, C_A	Unknown	$\ell_{cr}/d > 4.2$[f]
		—	C_N, C_m	—	No Data
		—	$C_{m_q} + C_{m_{\dot{\alpha}}}$	—	No Data
Slender Cones with Bulbous Bases	Subsonic	—	p_b, C_A, C_N, C_m, $C_{m_q} + C_{m_{\dot{\alpha}}}$	—	No Data
	Transonic	—		—	
	Supersonic	—		—	
	Hypersonic	—		—	
High Drag Cones	Subsonic	—	p_b, C_A	—	
		—	C_N, C_m	—	
		—	$C_{m_q} + C_{m_{\dot{\alpha}}}$	—	
	Transonic	—	p_b, C_A	—	
	Transonic	—	C_N, C_m	—	

Suggested Sting Criteria[a] Concluded

Models	Mach Regime	Mach Number	Measurements	Boundary Layer[b]	Critical Sting Length, $\approx \ell_{cr}/d$
High Drag Cones	Transonic	---	$C_{m_q} + C_{m_{\dot{\alpha}}}$	---	No Data
	Supersonic	1.6 to 3	p_b, C_A	Unknown	4
		---	C_N, C_m	---	No Data
		---	$C_{m_q} + C_{m_{\dot{\alpha}}}$	---	
	Hypersonic	---	p_b, C_A	---	
		---	C_N, C_m	---	
		---	$C_{m_q} + C_{m_{\dot{\alpha}}}$	---	
Wing Configurations	Subsonic	0.6 to 0.9	p_b, C_A	Turbulent	$\ell_{cr}/d \geq 5$[f]
		---	C_N, C_m	---	No Data
		---	$C_{m_q} + C_{m_{\dot{\alpha}}}$	---	No Data
	Transonic	0.95 to 1.05	p_b, C_A	Turbulent	$\ell_{cr}/d \geq 5$[f]
		1.1 to 1.3	p_b, C_A	Turbulent	2
		---	C_N, C_m	---	No Data
		---	$C_{m_q} + C_{m_{\dot{\alpha}}}$	---	
	Supersonic	---	p_b, C_A	---	
		---	C_N, C_m	---	
		---	$C_{m_q} + C_{m_{\dot{\alpha}}}$	---	
	Hypersonic	---	p_b, C_A	---	
		---	C_N, C_m	---	
		---	$C_{m_q} + C_{m_{\dot{\alpha}}}$	---	
Sliced Base Configuration	Subsonic	---	p_b, C_A, C_N, C_m, $C_{m_q} + C_{m_{\dot{\alpha}}}$	---	No Published Data
	Transonic	---		---	
	Supersonic[h]	---		---	
	Hypersonic	---		---	

NOTES:

[a] Criteria for $\alpha = 0$ for p_b, $C_{m_q} + C_{m_{\dot{\alpha}}}$, C_A.

[b] Boundary-layer condition generally at model base.

[c] ℓ_{cr}/d strongly dependent on Re_{ℓ}.

[d] Available data are not sufficient for indicating specific critical sting lengths. Stings with effective sting lengths greater than the value shown are interference-free of length effects.

[e] Similar tests as reported herein tentatively scheduled for 1978 at $M_\infty = 1.5$, 5, and 8.

[f] Available data are not sufficient for indicating specific critical sting lengths. Stings with effective sting lengths less than the value shown will have interference effects.

[g] ℓ_{cr}/d possibly frequency dependent.

[h] Tests will be conducted in 1977.

3.0 APPARATUS

3.1 Wind Tunnel

Tunnel A is a continuous, closed-circuit, variable-density wind tunnel with an automatically driven flexible-plate-type nozzle and a 40- by 40-in. test section. The tunnel can be operated at Mach numbers from 1.5 to 6 at maximum stagnation pressures from 29 to 200 psia, respectively, and stagnation temperatures up to 750°R (M_∞ = 6). Minimum operating pressures range from about one-tenth to one-twentieth of the maximum at each Mach number. The tunnel is equipped with a model injection system which allows removal of the model from the test section while the tunnel remains in operation. Details of the wind tunnel and model injection system are shown in Fig. 1.

3.2 Model

The stainless-steel model (Fig. 2) was a blunt 7-deg half-angle cone with a base diameter of 8 in. The bluntness ratio (r_n/r_b) was 0.15, and the moment reference point (also pivot axis location) was located at 60.9 percent of the model length aft of the model nose. The model was balanced to locate the center of gravity on the balance pivot axis.

Figure 3 shows the location of the surface and base pressure taps. The surface pressure was measured close to the model shoulder (Fig. 3a) and was on the leeward side for positive angles of attack. The location of the base pressure tap was on a 0.93-in. radius for the $\omega d/2V_\infty$ = 0.0033 tests (Fig. 3b) and 2.86-in. radius for the $\omega d/2V_\infty$ = 0.0056 tests (Fig. 3c). The tap location was changed for the $\omega d/2V_\infty$ = 0.0056 tests since the base pressure showed no variation with oscillation amplitude (θ) during the $\omega d/2V_\infty$ = 0.0033 tests.

3.3 Test Mechanism and Interference Hardware

The VKF-1.C pitch-/yaw-damping test mechanism (Fig. 4) utilizes a cross-flexure pivot, an electric shaker motor, and a one-component moment beam which is instrumented with strain gages to measure the forcing moment of the shaker motor. The motor is coupled to the moment beam by means of a connecting rod and flexural linkage which converts the translational force to a moment to oscillate the model at amplitudes up to ±3 deg (depending on flexure balance)

and frequencies from 2 to 20 Hz. The cross flexures, which are instrumented to measure the pitch/yaw displacement, support the model loads and provide the restoring moment to cancel the inertia moment when the system is operating at the natural frequency. Since the moment beam (which is used to measure the forcing moment) is not subjected to the static loads, it can be made as sensitive as required for the dynamic measurements. A pneumatic- and spring-operating locking device is provided to hold the model during injection into or retraction from the tunnel. Figure 5 shows photographs of the test mechanism.

The cross-flexure balance of the VKF-1.C mechanism is supported by a long slender sting so that large effective sting lengths (ℓ_s) and small effective sting diameters (d_s) can be obtained, which will eliminate or certainly minimize sting interference effects. The present model when mounted to the VKF-1.C test mechanism had an effective sting length of 3.45 model diameters and an effective sting-to-model diameter ratio of 0.22. This sting configuration was used during the present $\omega d/2V_\infty = 0.0033$ tests and also during the Ref. 22 tests. For the present interference study, the effective sting length was shortened by positioning a conical flare (Figs. 6 and 7) at 3.3 (Fig. 6a), 2.5, 2, and 1 (Fig. 6b) model diameters to the rear of the model base. The flare was mounted to the motor housing such that it did not touch the sting forward of the motor housing. This eliminated the possibility of the flare changing the sting frequency characteristics or model tare damping. The plates were attached to the flare (Figs. 6c, d, and e) and also did not touch the sting. Model support details are shown in Fig. 7 and plate details in Fig. 8.

3.4 Instrumentation

3.4.1 Tunnel

Tunnel A stilling chamber pressure is measured with a 15-, 60-, 150-, or 300-psid transducer referenced to a near vacuum. Based on periodic comparisons with secondary standards, the uncertainty (a bandwidth which includes 95 percent of residuals) of the transducers is estimated to be within ±0.2 percent of reading or 0.015 psi, whichever is greater. Stilling chamber temperature is measured with a copper-constantan thermocouple with an uncertainty of ±3°F based on repeat calibration.

3.4.2 Model Pressure Measurements

The model base and shoulder pressures were measured using the standard pressure system in conjunction with fast response transducers which were attached to the sting system inside the model base. The standard pressure system consisted of 15-psid transducers referenced to a near vacuum and were used to measure steady-state pressures, while the 5-psid fast-response transducers were used to measure the transient pressure (the delta from the steady-state pressure) when the model was oscillating. Based on periodic comparisons with secondary standards, the uncertainties of the 15-psid transducers are estimated to be within ±0.15 percent of pressure or ±0.003 psia whichever is greater. Since the 5-psid fast-response transducers measured a delta pressure, their uncertainty is considered to be negligible.

The response characteristics of the fast response transducers were measured by applying a step input voltage and monitoring the transducer's output as a function of time. The tubing which connected the transducer to the model was also included in the laboratory tests. The maximum lag time was found to be 0.013 sec, and the periods for the two test frequencies were 0.18 and 0.3 sec.

3.4.3 Forced Oscillation

The forced-oscillation instrumentation (Ref. 35) utilizes an electronic analog system with precision electronics. The control, monitor, and data acquisition instrumentation are contained in a portable console that can be easily interfaced with the instrumentation of the various tunnels.

The control instrumentation provides a system which can vary the oscillation frequency, oscillation amplitude, and angular position of the model within the flexure limits. The oscillation amplitude is controlled by an electronic feedback loop which permits testing of both dynamically stable and unstable configurations.

Data are normally obtained at or near the natural frequency of the model flexure system; however, the electronic resolvers used permit data to be obtained off resonance. All gages are excited by d-c voltages, and outputs are increased to optimum values by d-c amplifiers. Typical balance outputs from an oscillating model are composed of oscillatory components (OC) superimposed on static components (SC). These components are separated in the data system by bandpass and

lowpass filters. The SC outputs are sent directly to the tunnel scanner and computer which calculate the static moment coefficients and sting deflections. The OC outputs are input to the resolver instrumentation and precise frequency measuring instrumentation. The resolvers utilize very accurate analog electronic devices to process the OC signals and output d-c voltages. The output d-c voltages are porportional to the amplitude squared, the in-phase and quadrature (90 deg out-of-phase) balance components (forcing torque), and the in-phase and quadrature sting components. The resolver and frequency outputs are read by the tunnel scanner and sent to the computer. The frequency instrument controls the length of the data interval in increments from approximately 2 to 60 sec during which time the scanner reads each input approximately ten times per second. The average values of the reading are calculated by the computer, which then uses these average values to calculate the dynamic derivatives. The method used to reduce the data may be found in Refs. 35 and 36.

4.0 PROCEDURE

4.1 Test Conditions

Nominal tunnel conditions at which the tests were conducted are shown in Table 1, and the test summary is presented in Table 2.

4.2 Test Procedures

The model was oscillated at a constant amplitude of ±1 deg for the pitch-damping tests. The nominal reduced frequency parameters were 0.0033 and 0.0056 radians. The oscillating pressure data were obtained as a function of time while the model was oscillating at ±1 deg.

4.3 Precision of Data

Uncertainties (bands which include 95 percent of the calibration data) in the basic tunnel parameters (p_o, T_o, and M_∞) were estimated from repeat calibrations of the instrumentation and from repeatability and uniformity of the test section flow during tunnel calibrations. These uncertainties were used to estimate uncertainties in other free-stream properties using a Taylor series method of error propagation (Ref. 37). The estimated uncertainties are as follows:

Test Conditions		Uncertainty, percent						
M_∞	$Re_d \times 10^{-6}$	M_∞	p_o	T_o	p_∞	q_∞	V_∞	Re_d
2.69	0.27	±0.7	±0.7	±0.5	±3.0	±1.6	±0.4	±1.4
2.90	0.51		±0.3		±3.0	±1.7		±1.3
2.92	1.63		±0.2		±3.0	±1.7		±1.3
3.01	3.10		±0.2		±3.2	±1.8		±1.4
3.01	4.53		±0.2		±3.2	±1.8		±1.4

The balances were calibrated before and after the tests, and check calibrations were made during the test. Sting bending effects utilizing the technique illustrated in Ref. 38 were used in the data reduction. Uncertainties in the measurements of sting effects were included in the error analysis. Structural damping values were obtained at vacuum conditions before the tunnel entry to evaluate the still-air damping contribution. The uncertainties in the balance and data system were combined with uncertainties in the tunnel parameters assuming a Taylor series method of error propagation (Ref. 37) to estimate the precision of the aerodynamic damping coefficients. The estimated uncertainties are as follows:

	Uncertainty, percent	
$Re_d \times 10^{-6}$	$C_{m_q} + C_{m_{\dot{\alpha}}}$	$\omega d/2V_\infty$
0.25	±3.5	±0.4
1.63	±2.4	±0.4
4.53	±2.3	±0.4

The uncertainties in the pressure measurements based on the transducer uncertainty quoted in Section 3.4.2 are as follows:

Base Pressure

M_∞	$Re_d \times 10^{-6}$	ℓ_s/d	p_b, psia	Uncertainty, percent p_b	Uncertainty, percent p_b/p_∞
2.69	0.27	3.3	0.06	±5.0	±5.8
		1.0	0.09	±3.3	±4.5
2.92	1.63	3.3	0.16	±1.9	±3.6
		1.0	0.32	±0.9	±3.1
3.01	4.53	3.3	0.47	±0.6	±3.1
		1.0	0.89	±0.3	±3.0

Surface Pressure

M_∞	$Re_d \times 10^{-6}$	Uncertainty, percent p_s	Uncertainty, percent p_s/p_∞
2.69	0.27	±2.4	±3.8
2.92	1.63	±0.5	±3.0
3.01	4.53	±0.2	±3.0

Measurements of the model pitch angle are precise within ±0.05 deg, based on repeat calibrations. Model attitude corrections were made for model-balance deflections under air load, and the precision of the calculated model angle is estimated to be ±0.1 deg.

5.0 RESULTS AND DISCUSSION

A comparison of the damping data obtained with the standard VKF sting configuration (VKF-1.C, $\ell_s/d = 3.45$) and with the modified sting configuration (flare installed, $\ell_s/d = 3.3$) is presented in Fig. 9 for the two test frequencies. At the higher frequency (Fig. 9b), there is a mismatch in both Reynolds number and frequency. However, Uselton

(Ref. 21) and Ward (Ref. 39) showed that the pitch-damping derivatives for conical models at $\alpha = 0$ were generally independent of Reynolds number if the boundary-layer flow over the model base was either fully laminar or fully turbulent. For both Reynolds numbers in question, the flow over the model base was fully turbulent. In regard to the frequency mismatch, Uselton (Ref. 22) showed that, for a clean sting (zero or minimum interference) and a turbulent boundary layer at the model base, the damping derivatives at $\alpha = 0$ were independent of oscillation frequency. Uselton's results along with the present data are shown in Fig. 10. Although sufficient data are not available, the author believes that the same conclusion applies for laminar (Fig. 10a) and transitional (Fig. 10b) boundary layers at the model base. Therefore, it is evident from the results in Figs. 9 and 10 that the addition of the flare (Figs. 6 and 7) to the standard sting produced no measurable effects on the pitch-damping data.

The damping derivatives at $\alpha = 0$ are presented in Fig. 11 as a function of effective sting length ratio for laminar, transitional, and turbulent boundary layers at the model base. The data were obtained for reduced frequencies of 0.0033 and 0.0056. The damping derivatives for each type of boundary layer were essentially invariant with effective sting length for the range of 2 to 3.3 model diameters. Reducing the effective sting length to one model diameter generally increased model damping significantly, thereby indicating support interference due to sting length. The results show that the critical sting length as defined by the measurement of the pitch-damping derivatives for laminar, transitional, and turbulent boundary layer at the model base is 2 model diameters. This means that, for $\ell_s/d \geq 2$, the support interference is zero or certainly a minimum (possible diameter effects). The large increase in damping for the transitional Reynolds number is the well-known trend reported by Uselton (Ref. 21) and Ward (Ref. 39). In Ref. 22, damping data were shown essentially for the same model and test conditions as the present results. The data indicated that the critical sting length was 3 model diameters; however, the flare was attached to the sting for the $\ell_s/d = 2.3$ data, and therefore, those data may be in error.

Figure 12 shows the effect of Reynolds number and effective sting length on base pressure measurements at $\alpha = 0$. The base pressure trends with Reynolds numbers (Fig. 12a) are the typical trends reported by Whitfield (Ref. 1), which were discussed in Section 2.0 of this report. The two base pressure tap locations investigated showed essentially no effect of location and these results agree with those of Kavanau

(Ref. 4) and Cassanto (Ref. 12). In Fig. 12b, the base pressure trends with effective sting length are very similar to the damping trends with effective sting length. The base pressure increases significantly for small effective sting lengths ($\ell_s/d = 1$) for each type of boundary layer. The critical sting length for the transitional boundary layer is seen to be two model diameters; the same as was determined by the measurement of the damping derivatives. However, the base pressure measurements for the laminar and turbulent boundary layers indicate a critical sting length of 2.5 model diameters instead of two as was determined by the damping trends. Therefore, it is evident from these results that different interference indicators can produce different critical sting lengths.

The effect of the plates on the damping derivatives and base pressures for the clean ($\ell_s/d = 3.3$) and interference ($\ell_s/d = 1$) stings are presented in Figs. 13 and 14 for reduced frequencies of 0.0033 and 0.0056, respectively. In general, the addition of the plates to the clean sting configuration produced little effect on the damping derivatives and increased the base pressure slightly. The base pressure effect is opposite of that reported by Clay and Walchner (Ref. 29) at $M_\infty = 14$. The addition of Plate 1 to the interference sting generally decreased the level of interference (≈12 percent maximum) and increased the base pressure slightly. The plate results should be very helpful in the design of long slender stings for they indicate that a thin rib could be run along the top and bottom of the sting to increase the stiffness significantly and thereby eliminating or reducing the level of the sting bending corrections required for dynamic data.

The surface pressure measured close to the shoulder of the model at $\alpha = 0$ is shown in Fig. 15 as a function of model oscillation for different boundary layers. The sting configuration was the clean sting ($\ell_s/d = 3.3$). The laminar and turbulent data showed typical pressure trends with model oscillation. The transitional data displayed typical trends for the negative oscillation angles; however, for $\theta \approx 0.8$ to 1.0 deg, there was a sudden rise in the pressure. As the model moved on the downswing from $\theta = 1$ deg toward $\theta = 0$, then the pressure decreased until $\theta \approx 0.3$ deg where the level obtained was that measured during the upswing from $\theta = 0$ to $\theta = 1$ deg. It is obvious that the transitional data have a pressure hysteresis loop at the positive angles of attack. In an effort to try to explain this trend, Fig. 16 was prepared. The laminar and transitional data were corrected to Mach number 3 by inviscid pressure relationships and then plotted along with the turbulent data. For clarity, only one cycle of data was plotted. From Fig. 16, it is evident that the transitional pressure rise actually

increased above the turbulent pressure level. The explanation for this trend is probably the fact that, as the model pitches to positive angle of attack, the leeside transition location moves toward the model nose (a typical trend for positive α) and the turbulent or near turbulent wake moves upon the rear portion of the model. This observation is somewhat substantiated if the pressure distribution is estimated by inviscid cone theory with the cone angle being modified by the boundary-layer displacement thickness. The theoretical results (Fig. 17) showed that a peak pressure occurred in the region where boundary-layer transition ended. This peak pressure was somewhat higher than the pressure for fully turbulent flow at the model base. The theory then seems to predict the experimental transition pressure rise which is shown in Fig. 16. However, the difference between the transition peak pressure and the fully turbulent pressure level was not predicted. The predicted pressure for the turbulent boundary layer agreed well with the experimental data. This trend of peak pressure near the end of transition was also reported by Laufer and Marte (Ref. 40) for a flat plate at $M_\infty = 2.55$.

Figure 18 shows the effect of sting length on the surface and base pressures at $\alpha = 0$ for laminar, transitional, and turbulent boundary layers at the model base. Decreasing the effective sting length ratio (ℓ_s/d) from 3.3 to 1 slightly increased the surface pressure for each type of boundary layer. It is unknown whether this small increase ($\approx$3 percent maximum) in surface pressure was sufficient to produce changes in the levels of the damping data as was shown in Fig. 11. The base pressures were generally constant with model oscillation, and the interference sting configuration ($\ell_s/d = 1$) produced much higher base pressures than the clean sting configuration ($\ell_s/d = 3.3$).

6.0 CONCLUSIONS

The critical sting length at $\alpha = 0$ was determined by the measurement of pitch-damping derivatives for laminar, transitional, and turbulent boundary layers at the model base. The effects of wedge plates on pitch damping and surface pressure measurements near the model shoulder as a function of model oscillation for a clean and an interference sting were also investigated. Data were obtained at Mach number 3 on a blunt 7-deg half-angle cone for reduced frequencies of 0.0033 and 0.0056. Reynolds number, based on model base diameter, ranged from 0.3×10^6 to 4.6×10^6. Conclusions based on these results are given below:

1. The critical sting length determined by the measurements of pitch-damping derivatives is 2.0 model diameters for the two reduced frequencies investigated and is independent of the type of boundary layer at the model base.

2. The critical sting length determined by base pressure measurements is approximately 2.5 model diameters.

3. In general, the addition of the wedge plates behind the model produced no effect on the damping data, thereby encouraging the incorporation of thin rib stiffeners in the design of long slender stings.

4. Decreasing the effective sting length to 1 model diameter increases the model base pressure substantially and the model surface pressure slightly.

7.0 FUTURE PROGRAMS

The fiscal year 1977 program involves investigation of sting length and diameter effects on pressure measurements in the model base region of a blunt 6-deg cone with a sliced base. These wind tunnel tests will be conducted at both supersonic and hypersonic Mach numbers. The 1977 program also includes free-flight damping data on the present 7-deg cone at supersonic Mach numbers for the purpose of obtaining interference-free data for comparison with the 1976 sting supported data (present results). Tentatively, it is planned to obtain data similar to that reported herein at the additional Mach numbers of 1.5, 5, and 8 in fiscal year 1978. Free-flight damping tests will also be conducted at $M_\infty = 8$ in 1978. The 1978 program combined with the 1976 and 1977 programs will provide data for the evaluation of sting support effects on base pressure measurements, surface pressure measurements (at model base), static-force coefficients (C_m, C_N), and pitch-damping derivatives of a 7-deg cone for a Mach number range from 1.5 to 8.

REFERENCES

1. Whitfield, J. D. "Critical Discussion of Experiments on Support Interference at Supersonic Speeds." AEDC-TN-58-30 (AD201108), August 1958.

2. Pick, G. S. "Sting Effects in Hypersonic Base Pressure Measurements." Department of the Navy, Report AL-85, December 1971.

3. Crocco, L. and Lees, L. "A Mixing Theory for the Interaction between Dissipative Flows and Nearly Isentropic Streams." Journal of the Aeronautical Sciences, Vol. 19, No. 10, October 1952, pp. 649-676.

4. Kavanau, L. L. "Results of Some Base Pressure Experiments at Intermediate Reynolds Numbers with $M_\infty = 2.84$." Report No. HE-150-117, October 1953.

5. Perkins, Edward W. "Experimental Investigation of the Effects of Support Interference on the Drag of Bodies of Revolution at a Mach Number of 1.5." NACA TN 2292, February 1951.

6. Reller, J. O., Jr. and Hamaker, F. M. "An Experimental Investigation of the Base Pressure Characteristics of Nonlifting Bodies of Revolution at Mach Numbers from 2.73 to 4.98." NACA TN 3393, March 1955.

7. Sevier, K. R. and Bogdonoff, S. M. "The Effect of Support Interference on the Base Pressure of a Body of Revolution at High Reynolds Numbers." Report No. 332, AFOSR TN 55-301, October 1955.

8. Chapman, D. R. "An Analysis of Base Pressure at Supersonic Velocities and Comparison with Experiment." NACA TN 2137, July 1950.

9. Reichenau, D. E. A. "Sting and Strut Support Interference Effects on a Cylindrical Model with an Ogive Nose at Mach Numbers from 0.4 to 1.4." AEDC-TR-72-175 (AD905771L), November 1972.

10. Reese, D. E., Jr. and Wehrend, W. R., Jr. "Effects of Sting-Support Interference on the Base Pressures of a Model Having a Blunt-Nosed Cylinder Body and a Conical Flare at Mach Numbers of 0.65 to 2.20." NASA TM X-161, February 1960.

11. Lee, George and Summers, James L. "Effects of Sting-Support Interference on the Drag of an Ogive-Cylinder Body with and without a Boattail at 0.6 to 1.4 Mach Number." NACA RM A57I09, December 1957.

12. Cassanto, J. M. "Base Pressure Results at M_∞ = 4 Using Free-Flight and Sting-Supported Models." AIAA Journal, Vol. 6, No. 7, July 1968.

13. Cassanto, J. M. "Radial Base-Pressure Gradients in Laminar Flow." AIAA Journal, Vol. 5, No. 12, December 1967.

14. Jaffe, P. "A Free-Flight Investigation of Transonic Sting Interference." NASA TM 33-704, January 1975.

15. Vlajinac, M., Stephens, T., Gilliam, G., and Pertsas, N. "Subsonic and Supersonic Static Aerodynamic Characteristics of a Family of Bulbous Base Cones Measured with a Magnetic Suspension and Balance System." NASA CR-1932, January 1972.

16. Adcock, J. B. "Some Experimental Relations between the Static and Dynamic Stability Characteristics of Sting-Mounted Cones with Bulbous Bases." Paper presented at the Third Technical Workshop on Dynamic-Stability Problems, Moffett Field, California, November 1968.

17. Fuller, D. E. and Langhans, V. E. "Effect of Afterbody Geometry and Sting Diameter on the Aerodynamic Characteristics of Slender Bodies at Mach Numbers from 1.57 to 2.86." NASA TN D-2042, November 1963.

18. Tunnell, P. J. "An Investigation of Sting Support Interference on Base Pressure and Forebody Chord Force at Mach Numbers from 0.60 to 1.30." NACA-RM-A54K16a, January 1955.

19. Ericsson, L. E. and Reding, J. P. "Aerodynamic Effects of Bulbous Bases." NASA CR-1339, August 1969.

20. Wehrend, W. R., Jr. "An Experimental Evaluation of Aerodynamic Damping Moments of Cones with Different Centers of Rotation." NASA TN D-1768, March 1963.

21. Uselton, B. L. "Investigation of Sting Support Interference Effects on the Dynamic and Static Stability Characteristics of a 10-deg Cone at Mach Numbers 2.5, 3.0, and 4.0." AEDC-TDR-64-226 (AD450660), November 1964.

22. Uselton, J. C., Uselton, B. L., and Helmlinger, K. R. "An Examination of the Small-Amplitude Dynamic Stability Test Technique." AEDC-TR-74-131 (ADA008477), April 1975.

23. Uselton, B. L. and Wallace, A. R. "Damping-in-Pitch and Drag Characteristics of the Viking Configuration at Mach Numbers from 1.6 through 3." AEDC-TR-72-56 (AD741826), May 1972.

24. Steinberg, S., Uselton, B. L., and Siemers, P. M. "Viking Pitch-Damping Derivatives as Influenced by Support Interference and Test Techniques." Journal of Spacecraft and Rockets, Vol. 10, No. 7, July 1973.

25. Sallet, D. W. "A Splitter Plate for the Prevention of Vortex Shedding behind Finite Circular Cylinders in Uniform Cross Flow." NOLTR 69-31, July 1967.

26. Roshko, A. "On the Drag and Shedding Frequency of Two-Dimensional Bluff Bodies." NACA TN 3169, July 1954.

27. Roshko, A. "On the Development of Turbulent Wakes from Vortex Streets." NACA R 1191, 1954.

28. Baughman, L. E. and Jack, J. R. "Experimental Investigation of the Effects of Support Interference on the Pressure Distribution of a Body of Revolution at a Mach Number of 3.12 and Reynolds Numbers from 2 x 10^6 to 14 x 10^6." NACA RM E53E28, August 1953.

29. Clay, J. T. and Walchner, O. "Nose Bluntness Effects on the Stability Derivatives of Cones in Hypersonic Flow." Transactions of the Second Technical Workshop on Dynamic Stability Testing, Vol. 1, Paper 8, Arnold Engineering Development Center, Arnold AFS, Tennessee, April 1965.

30. Love, E. S. "A Summary of Information on Support Interference at Transonic and Supersonic Speeds." NACA RM L53K12, January 1954.

31. Sieling, W. R. "The Effect of Sting Diameter and Length on Base Pressure at M = 3.88." The Aeronautical Quarterly, November 1968, pp. 368-374.

32. Peckham, D. H. "Exploratory Tests on Sting Interference at a Mach Number of 6-8." Tech Note AERO 2721, October 1960.

33. Trescot, C. D., Jr., Brown, C. A., Jr., and Howell, D. T. "Effects of Reynolds Number and Model Support on the Supersonic Aerodynamic Characteristics of a 140°-Included-Angle Cone." NASA TM X-3019, July 1974.

34. Hart, R. C. "Effects of Stabilizing Fins and a Rear-Support Sting on the Base Pressures of a Body of Revolution in Free Flight at Mach Numbers from 0.7 to 1.3." NACA-RM L52E06, September 1952.

35. Burt, G. E. "A Description of a Pitch/Yaw Dynamic Stability, Forced-Oscillation Test Mechanism for Testing Lifting Configurations." AEDC-TR-73-60 (AD762286), June 1973.

36. Schueler, C. J., Ward, L. K., and Hodapp, A. E., Jr. "Techniques for Measurements of Dynamic-Stability Derivatives in Ground Test Facilities." AGARDograph 121 (AD669227) October 1967.

37. Beers, Yardley. Introduction to the Theory of Error. Addison-Wesley Publishing Company, Inc., Reading, Massachusetts, 1957, pp. 26-36.

38. Burt, G. E. and Uselton, J. C. "Effect of Sting Oscillations on the Measurements of Dynamic Stability Derivatives." Journal of Aircraft, Vol. 13, No. 3, March 1976.

39. Ward, L. K. "Influence of Boundary-Layer Transition on Dynamic Stability at Hypersonic Speeds." Transactions of the Second Technical Workshop on Dynamic Stability Testing, Vol. II." Paper 6, April 1965.

40. Laufer, John and Marte, Jack E. "Results and a Critical Discussion of Transition-Reynolds-Number Measurements on Insulated Cones and Flat Plates in Supersonic Wind Tunnels." JPL -20-96, November 30, 1955.

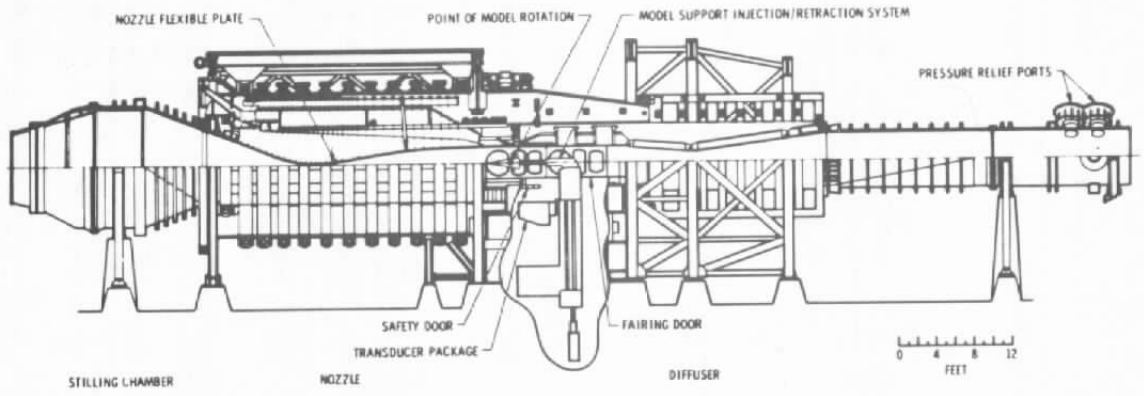

a. VKF Tunnel A

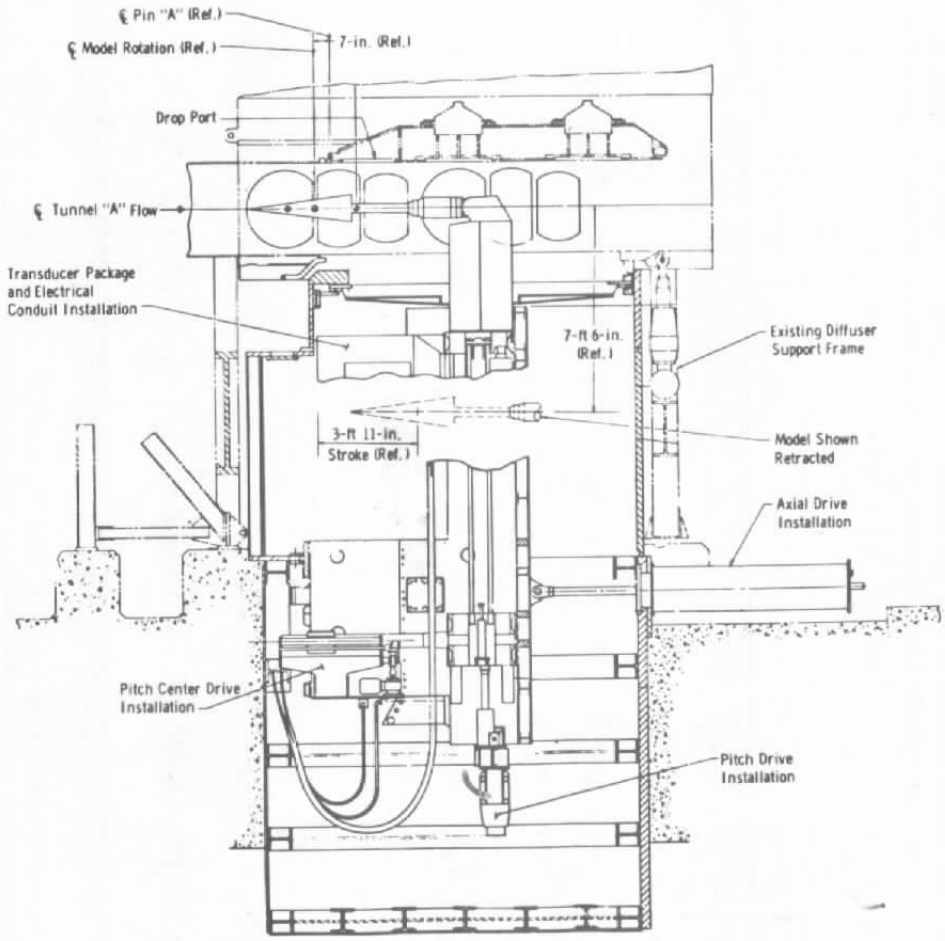

b. Model injection system

Figure 1. Wind tunnel and model injection system.

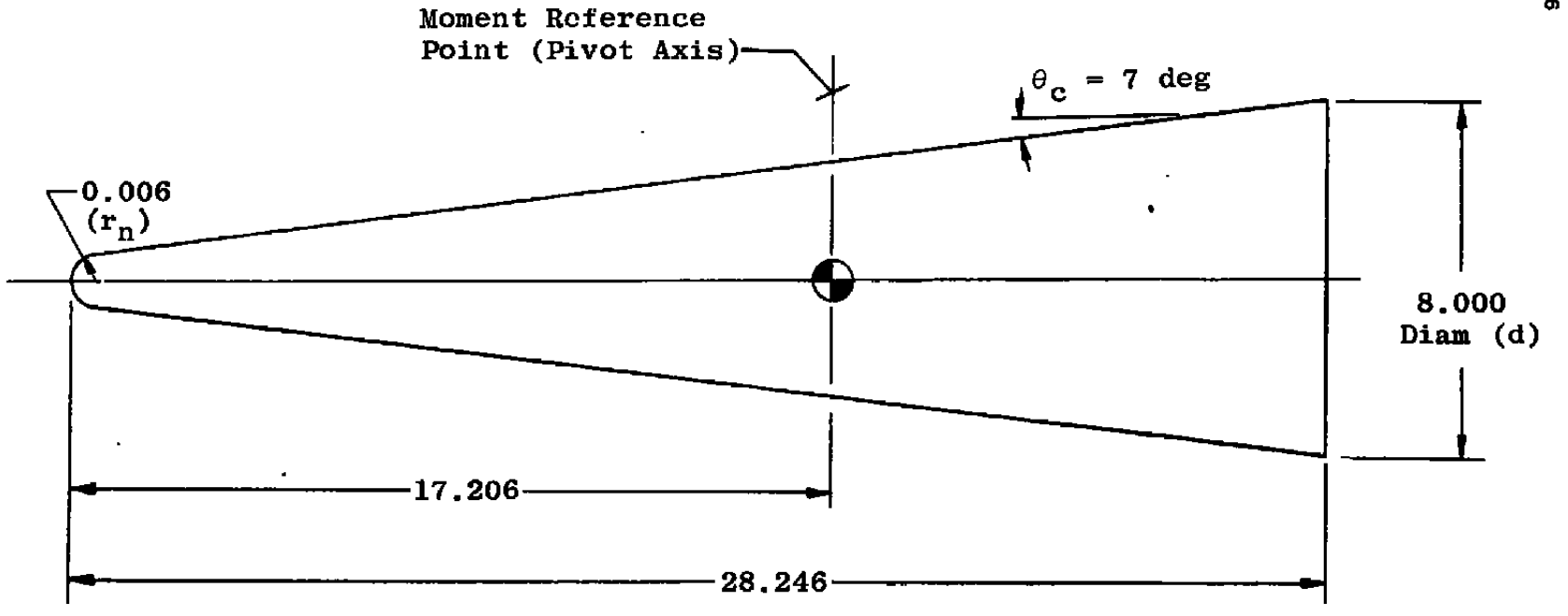

Figure 2. Model details.

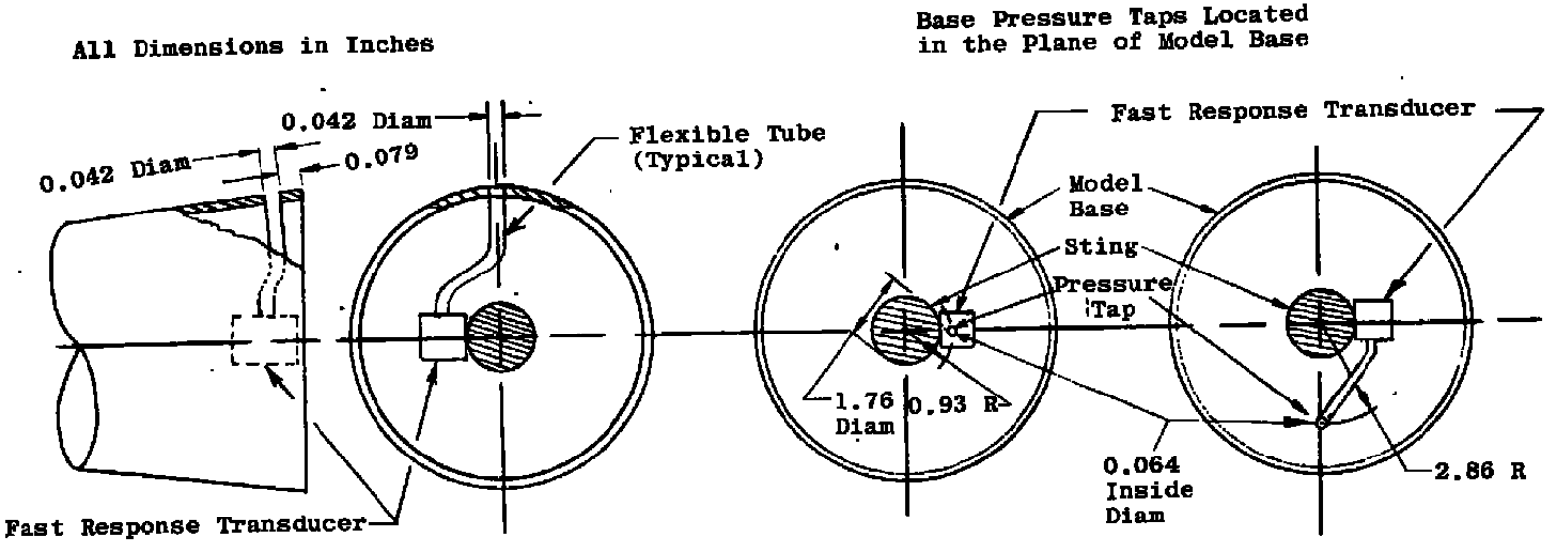

a. Surface pressure tap location

b. Base pressure tap location for $\omega d/2V_\infty = 0.0033$ test

c. Base pressure tap location for $\omega d/2V_\infty = 0.0056$ test

Figure 3. Location of pressure taps.

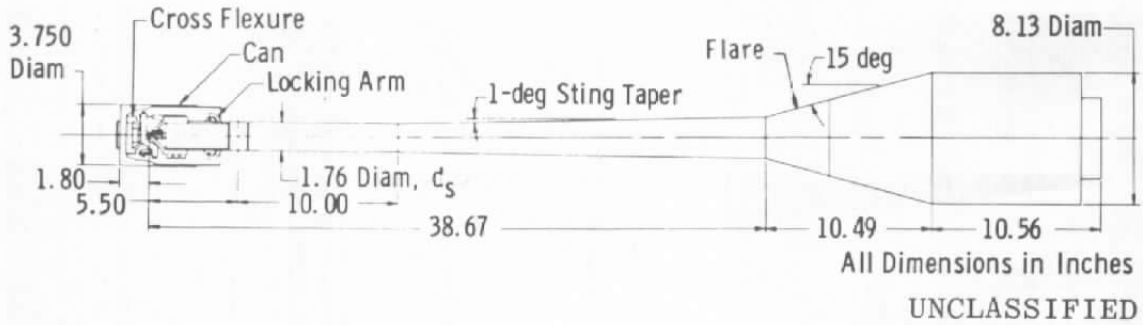

Figure 4. 1DOF test mechanism (VKF-1.C) details.

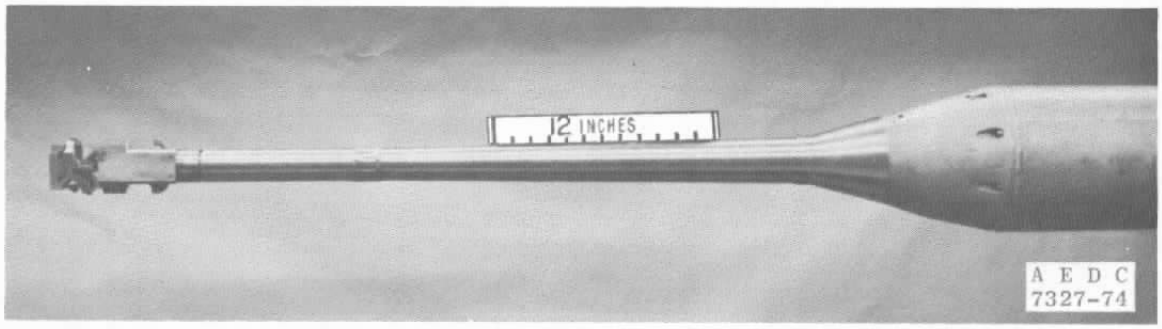

a. Forced-oscillation test mechanism

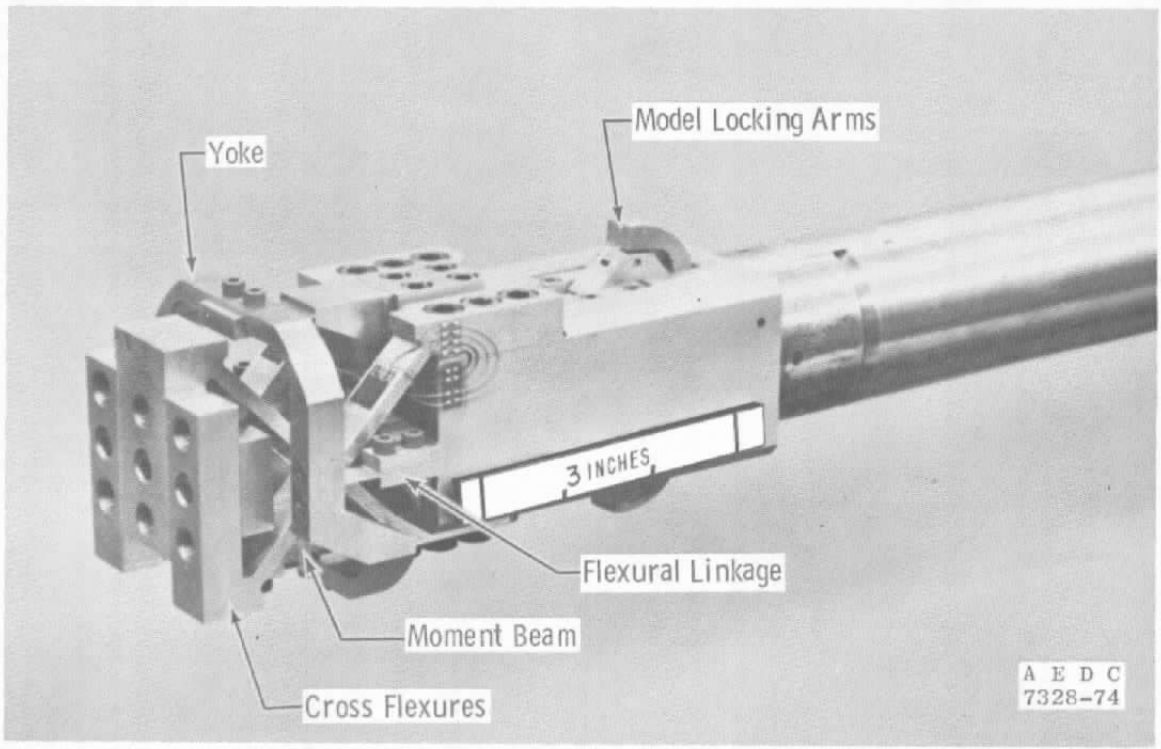

b. Cross-flexure balance

Figure 5. Photographs of 1DOF test mechanism (VKF-1.C).

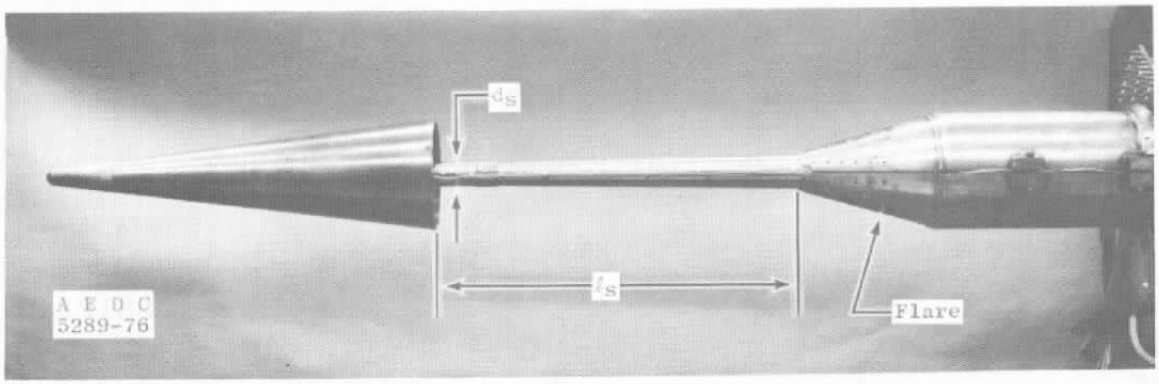

a. Clean sting, $\ell_s/d = 3.3$

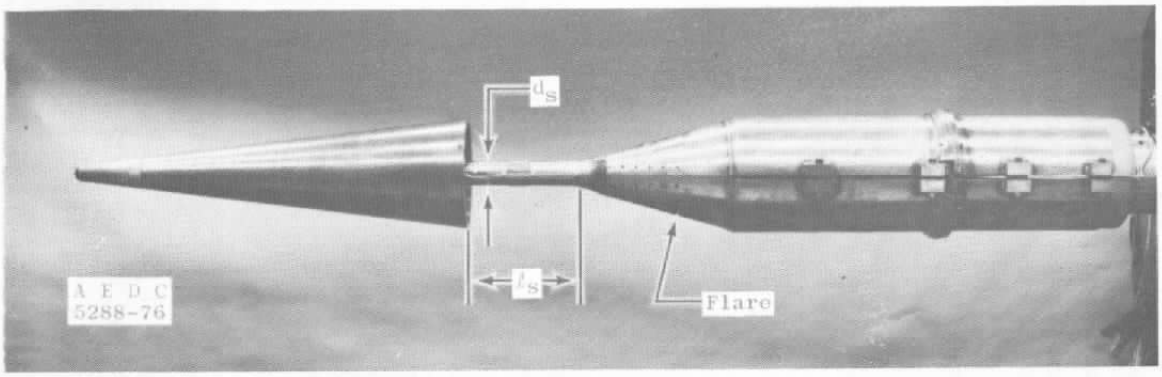

b. Interference sting, $\ell_s/d = 1$

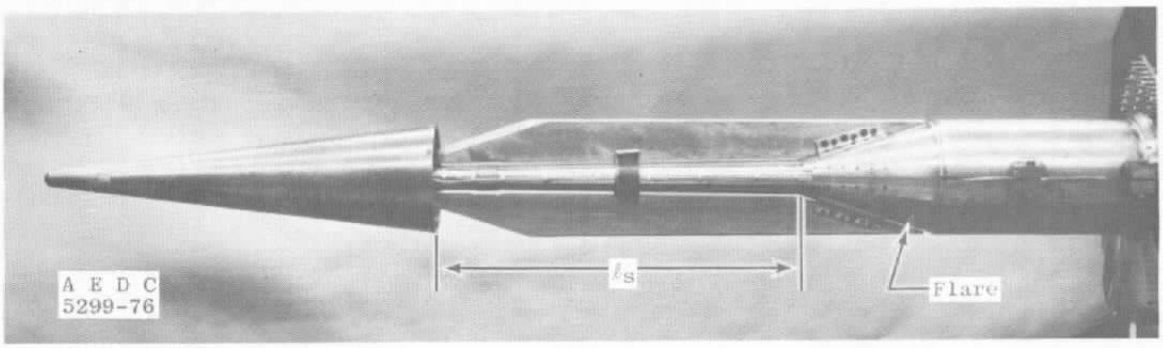

c. Plate installation, Plate 4, $\ell_s/d = 3.3$

Figure 6. Photographs of model support configurations.

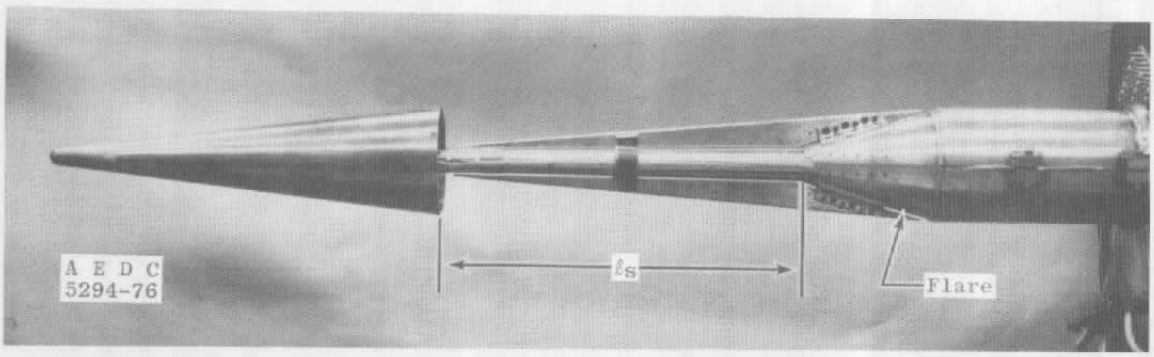

d. Plate installation, Plate 8, $\ell_s/d = 3.3$

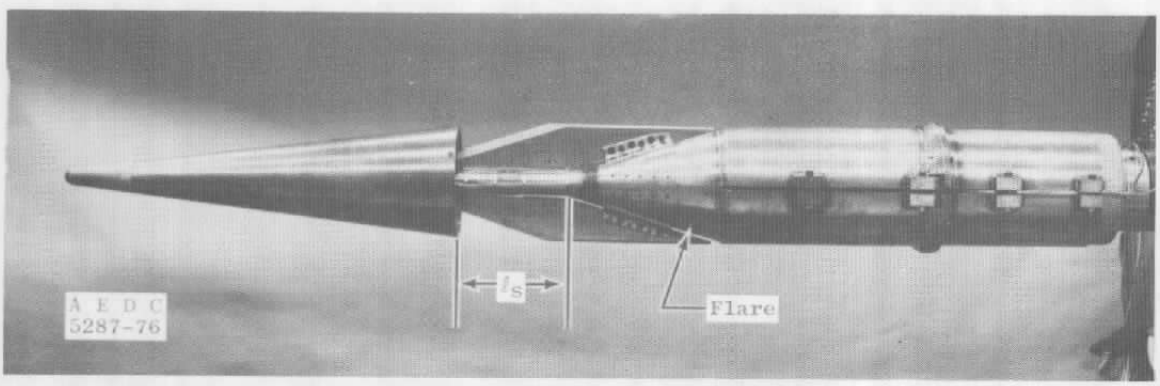

e. Plate installation, Plate 1, $\ell_s/d = 1$

Figure 6. Concluded.

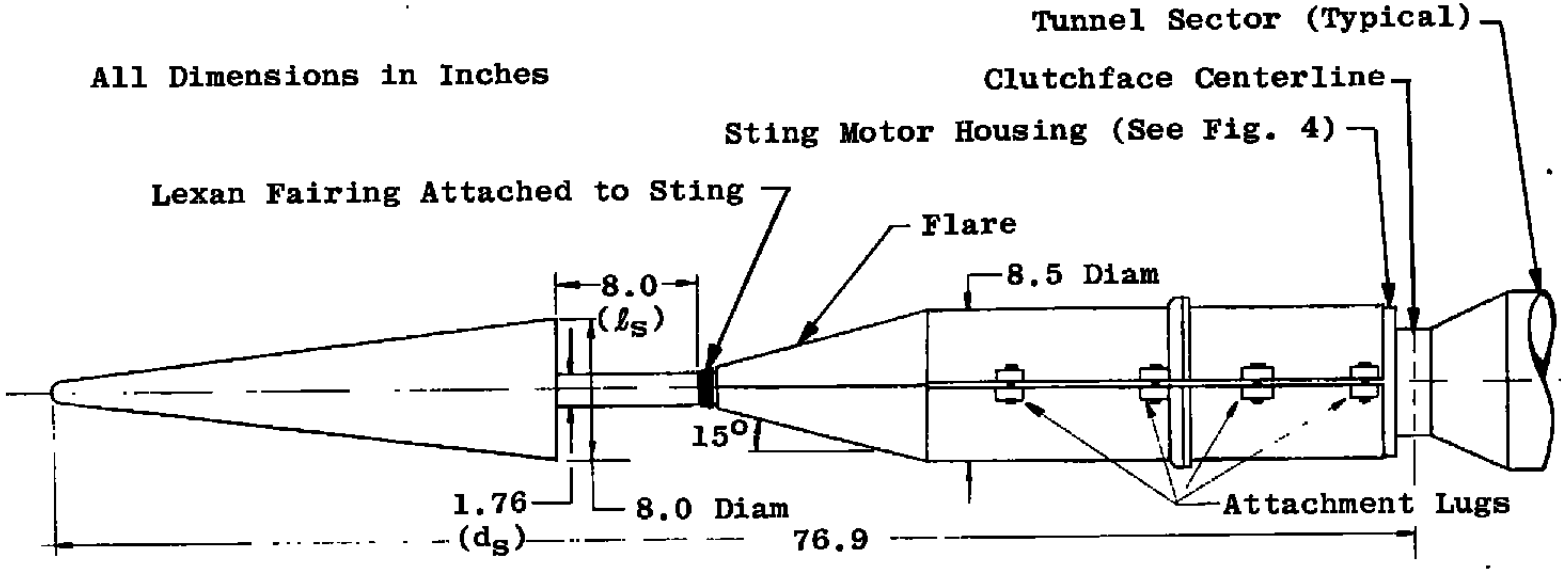

a. Interference sting, $\ell_s/d = 1$

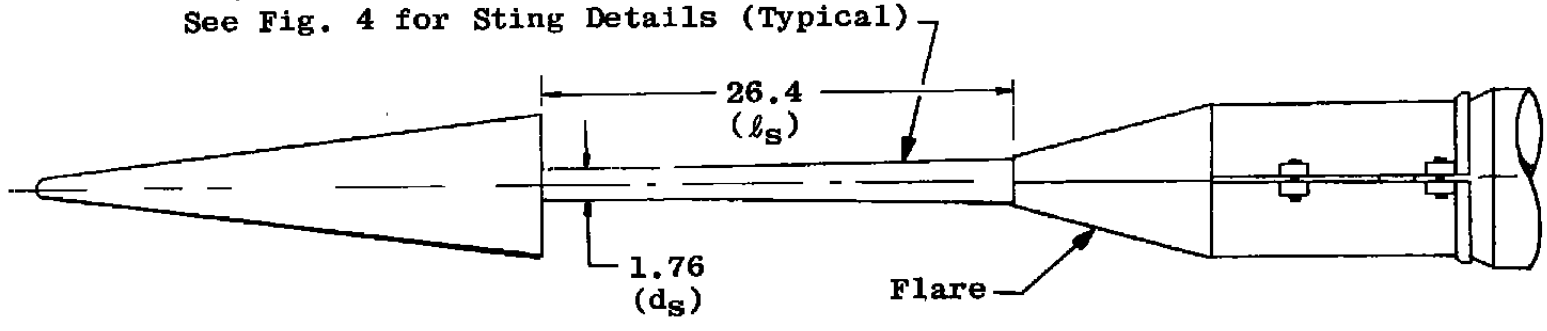

b. Clean sting, $\ell_s/d = 3.3$

Figure 7. Details of model support configurations.

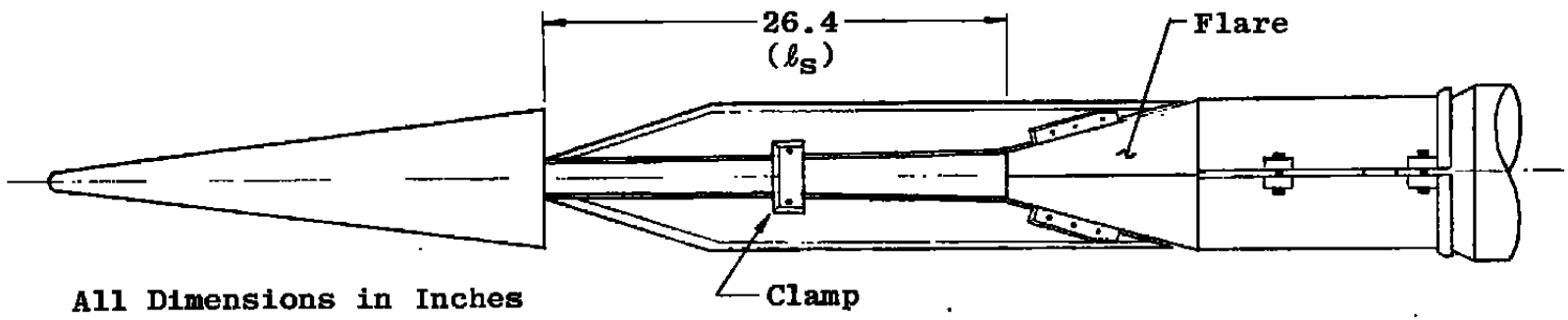

c. Plate 4 installed, $\ell_s/d = 3.3$

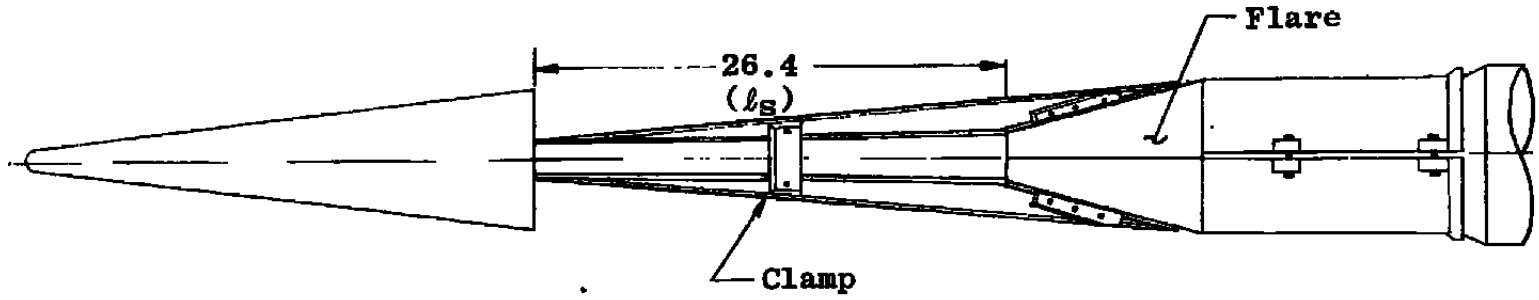

d. Plate 8 installed, $\ell_s/d = 3.3$

Figure 7. Continued.

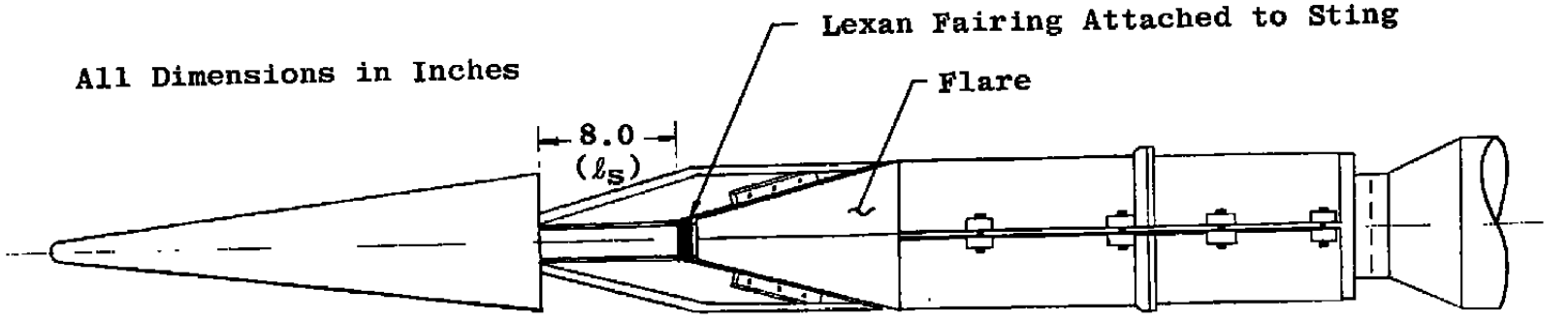

e. Plate 1 installed, $\ell_s/d = 1$

Figure 7. Concluded.

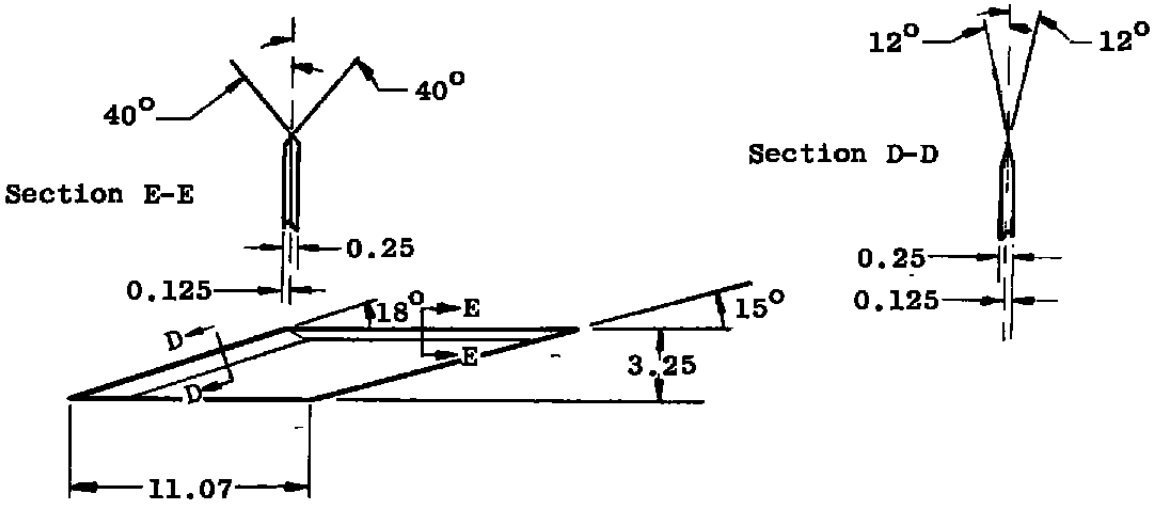

a. Plate 1

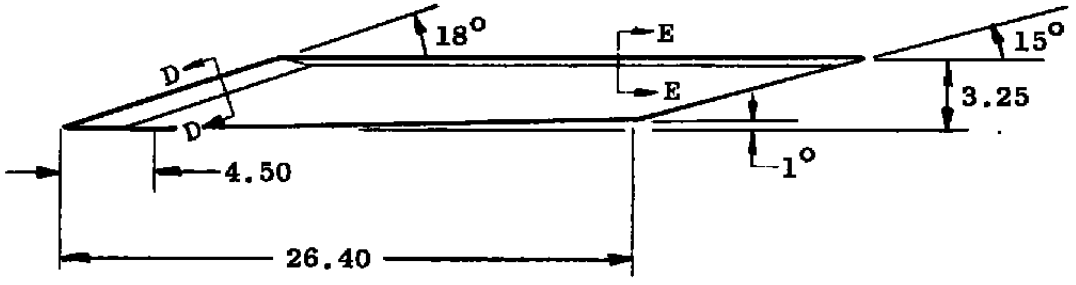

b. Plate 4

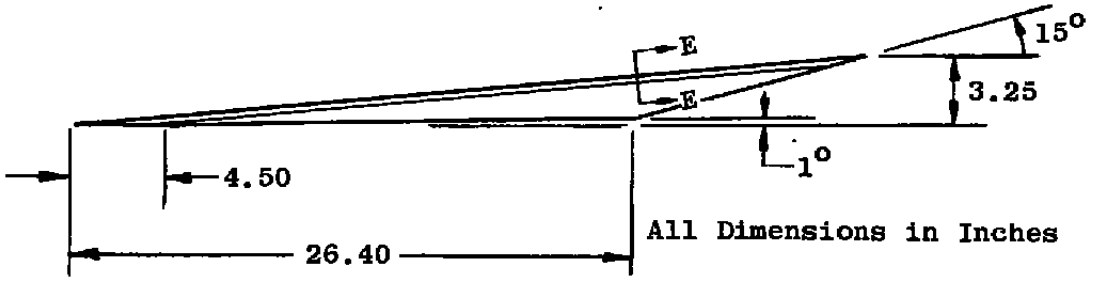

c. Plate 8

Figure 8. Plate details.

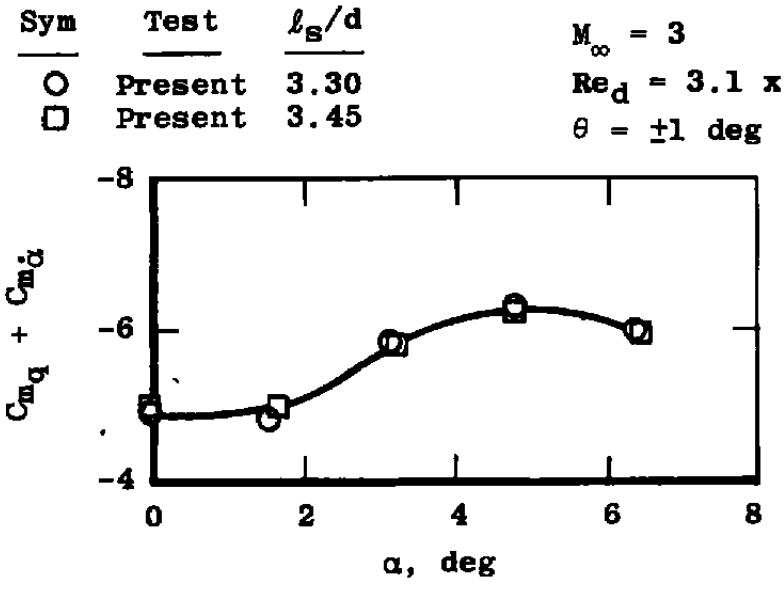

a. $\omega d/2V_\infty$ = 0.0033

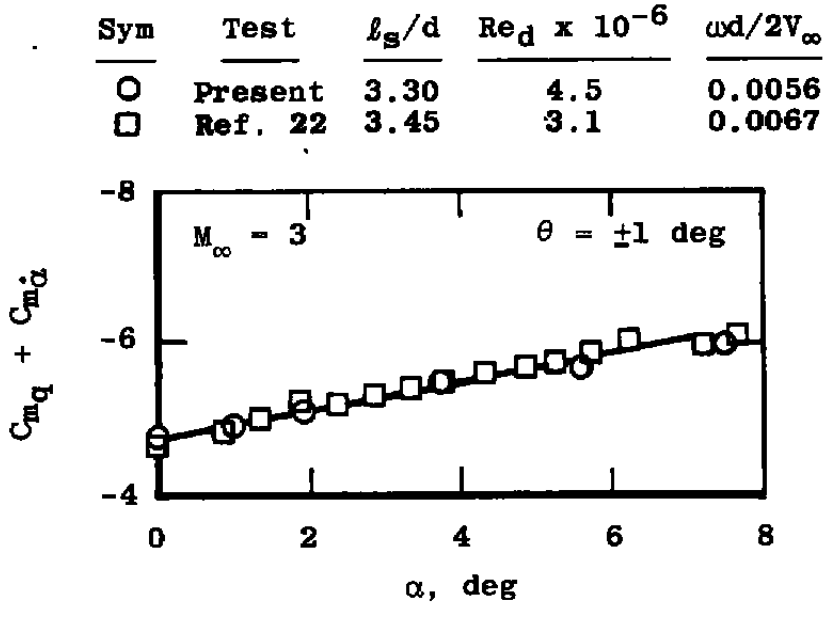

b. $\omega d/2V_\infty$ = 0.0056 and 0.0067

Figure 9. Effect of flare installation on the damping derivatives, d_s/d = 0.22.

Sym	Test	M_∞	$Re_d \times 10^{-6}$	ℓ_s/d	d_s/d
○	Present	2.7	0.3	3.3	0.22
□	Present	2.9	0.5	3.3	0.22

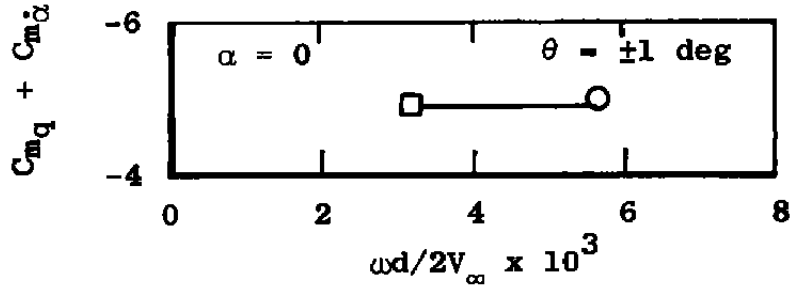

a. Laminar boundary layer

Sym	Test	M_∞	$Re_d \times 10^{-6}$	ℓ_s/d	d_s/d
○	Present	2.9	1.6	3.3	0.22
□	Present	3.0	1.7	3.3	0.22

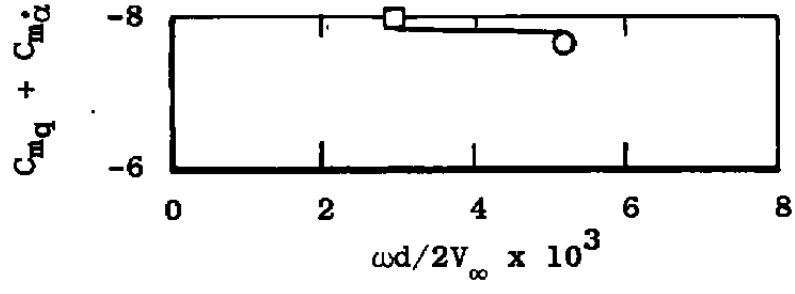

b. Transitional boundary layer

Sym	Test	M_∞	$Re_d \times 10^{-6}$	ℓ_s/d	d_s/d
○	Present	3.0	4.6	3.30	0.22
□	Ref. 22	3.0	3.1	3.45	0.22

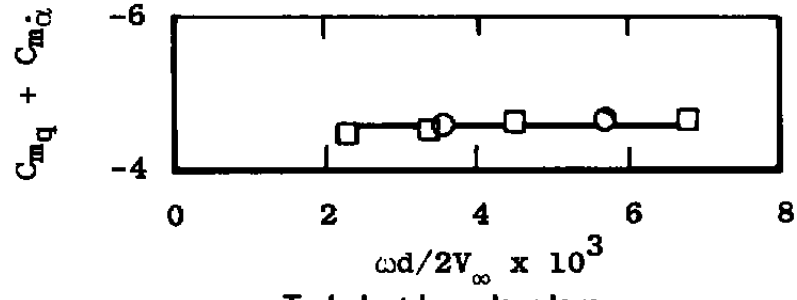

c. Turbulent boundary layer

Figure 10. Damping derivatives as a function of reduced frequency parameter for laminar, transitional, and turbulent boundary layer at the model base, $\alpha = 0$, $\theta = \pm 1$ deg.

Sym	Test	M_∞	$Re_d \times 10^{-6}$	Boundary Layer at Model Base
△	Present	2.9	≈0.4	Laminar
□	Present	3.0	≈1.7	Transitional
○	Present	3.0	≈4.5	Turbulent
◇	Ref. 22	3.0	≈3.1	Turbulent

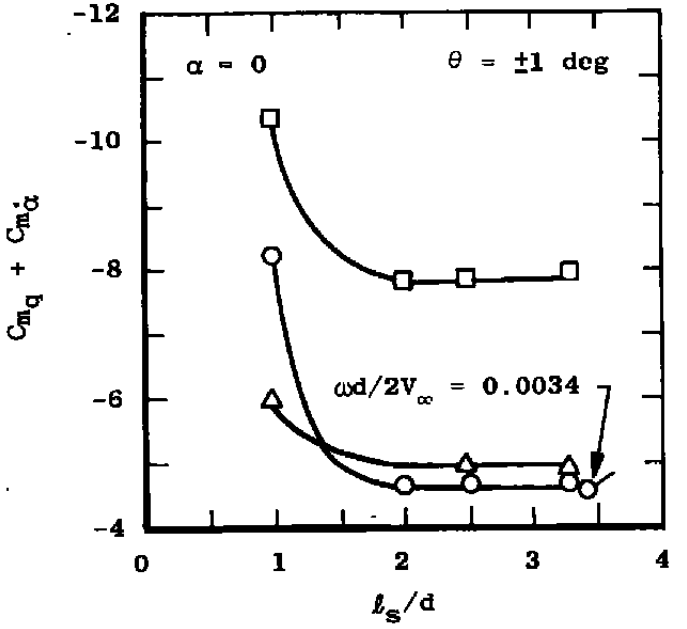

a. $\omega d/2V_\infty = 0.0033$

Sym	Test	M_∞	$Re_d \times 10^{-6}$	Boundary Layer at Model Base
△	Present	2.7	≈0.3	Laminar
□	Present	2.9	≈1.7	Transitional
○	Present	3.0	≈4.6	Turbulent
◇	Ref. 22	3.0	≈3.1	Turbulent

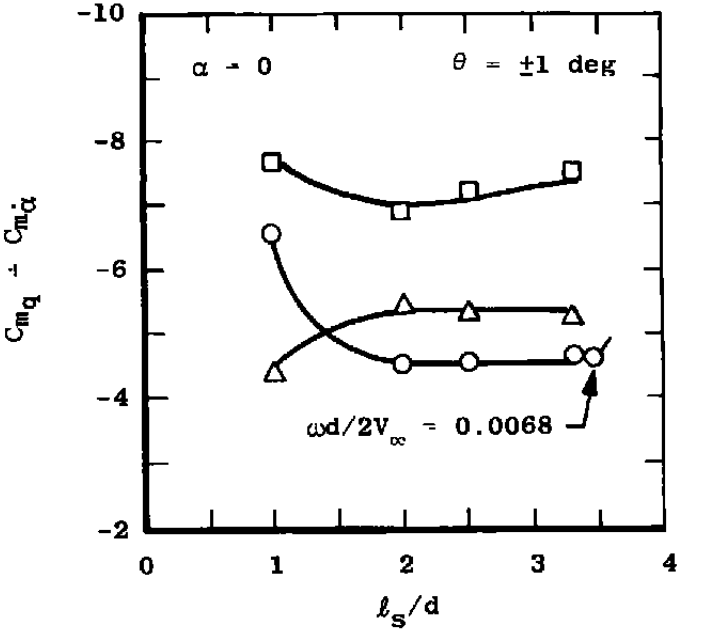

b. $\omega d/2V_\infty = 0.0056$

Figure 11. Damping derivatives as a function of effective sting length, $d_s/d = 0.22$.

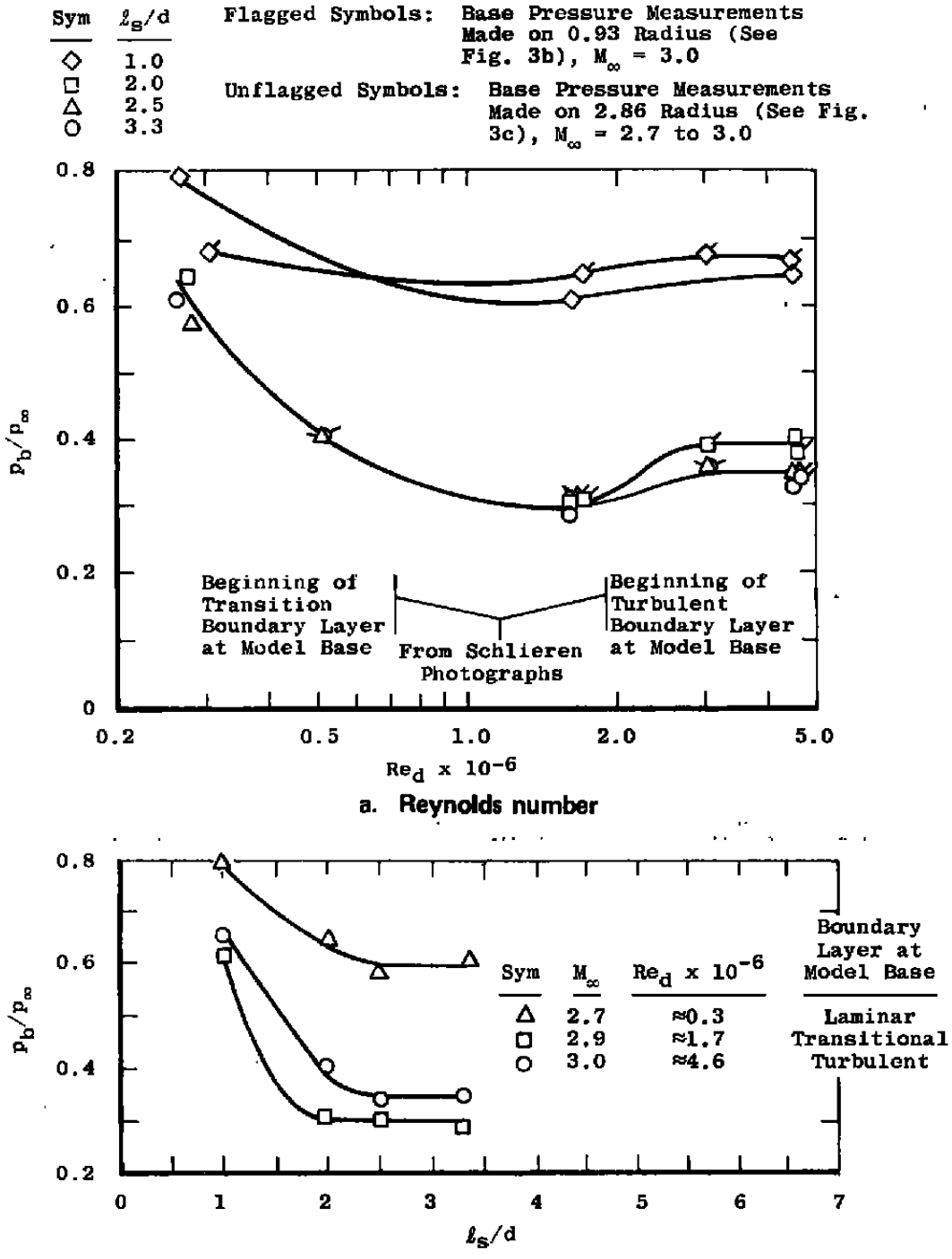

Figure 12. Base pressure as a function of Reynolds number and effective sting length, α = 0, d_s/d = 0.22.

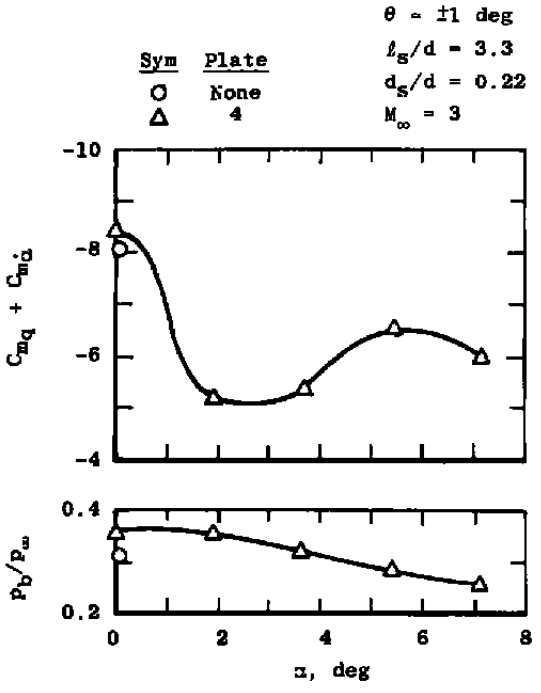

a. Plate 4, Re_d = 1.7 x 10^6

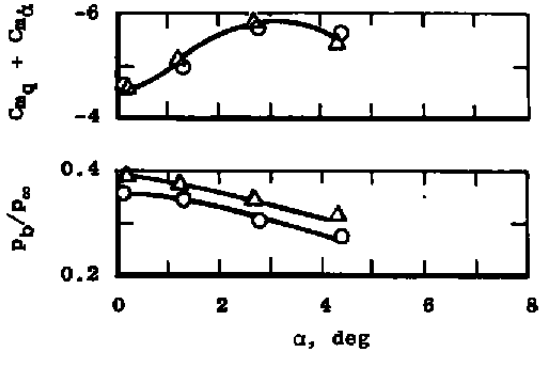

b. Plate 4, Re_d = 4.6 x 10^6

Figure 13. Effect of plates on damping derivatives and base pressure, $\omega d/2V_\infty$ = 0.0033.

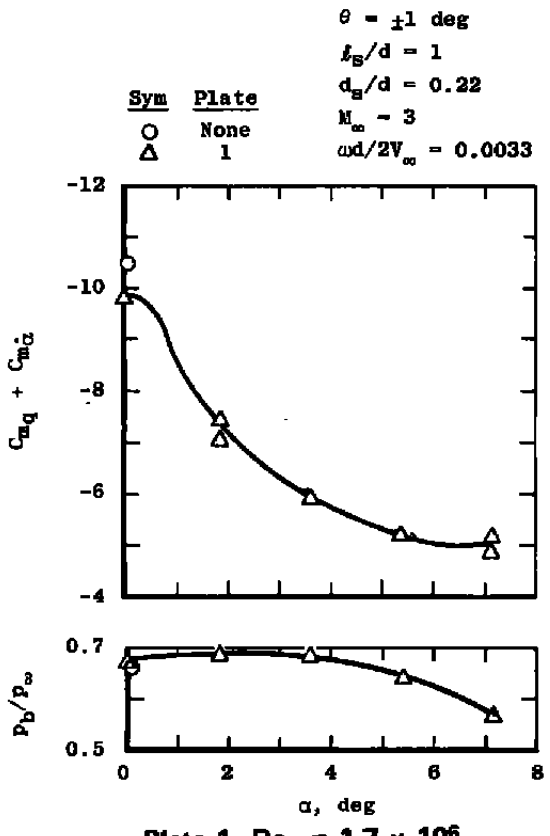

c. Plate 1, Re_d = 1.7 x 10^6

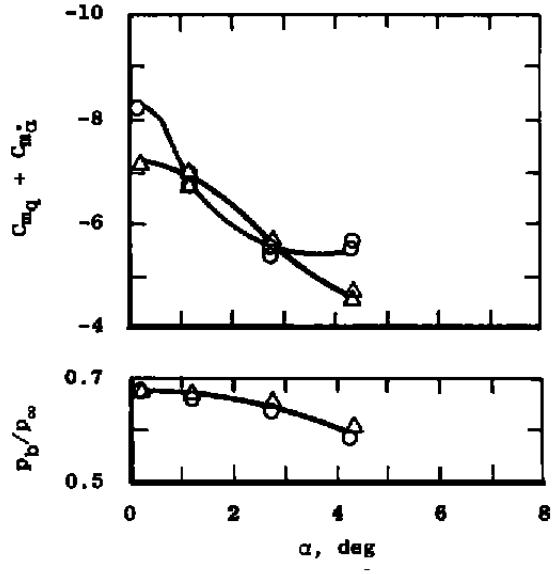

d. Plate 1, Re_d = 4.6 x 10^6

Figure 13. Concluded.

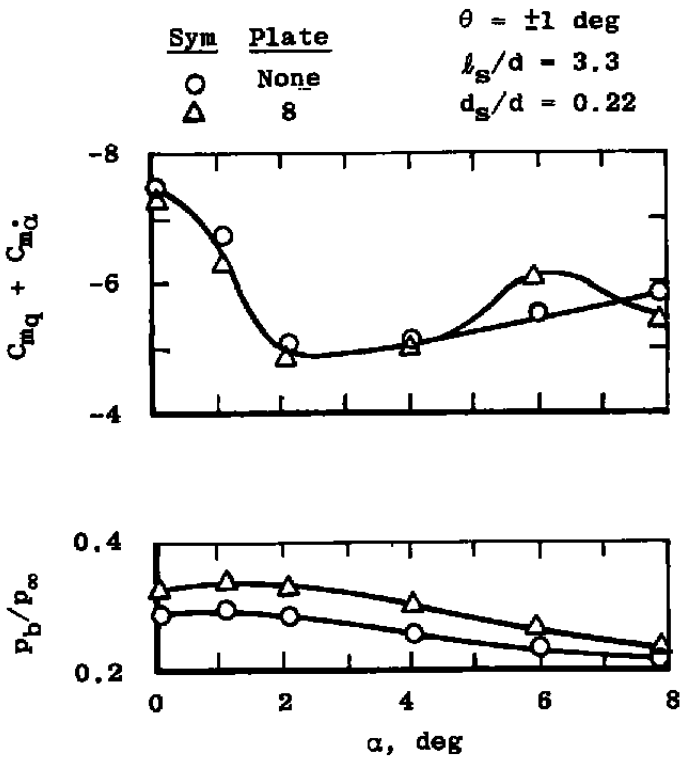

a. Plate 8, $Re_d = 1.6 \times 10^6$, $M_\infty = 2.9$

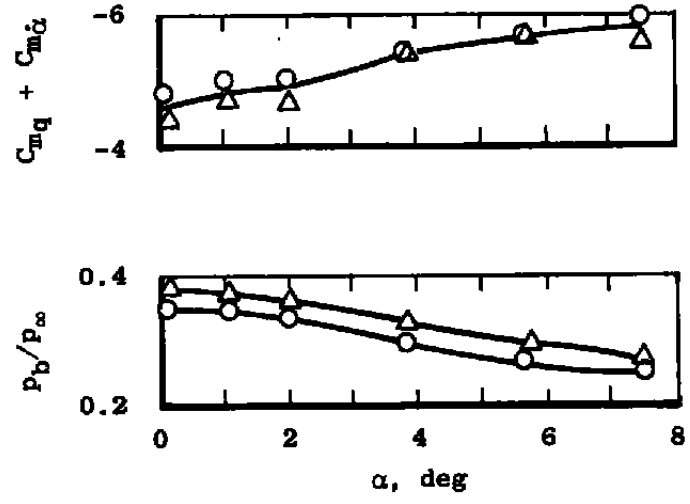

b. Plate 8, $Re_d = 4.5 \times 10^6$, $M_\infty = 3.0$

Figure 14. Effect of plates on damping derivatives and base pressure, $\omega d/2V_\infty = 0.0056$.

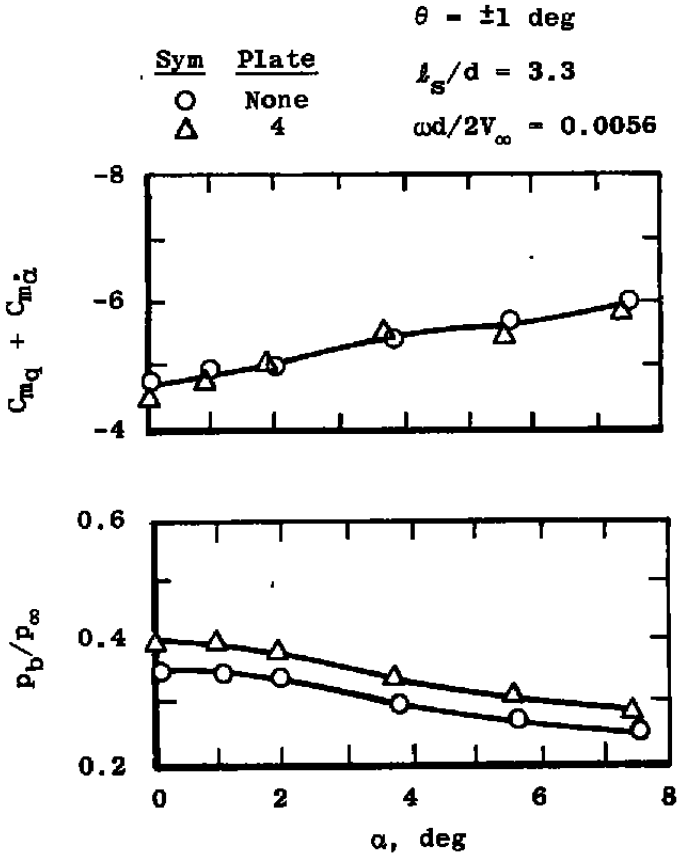

c. Plate 4, Re_d = 4.6 x 10^6, M_∞ = 3.0
Figure 14. Continued.

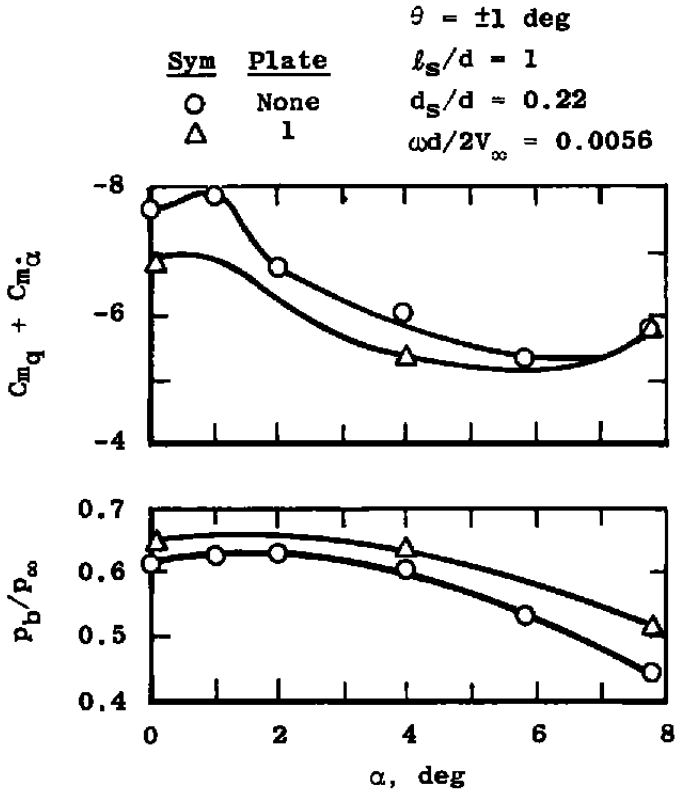

d. Plate 1, $Re_d = 1.7 \times 10^6$, $M_\infty = 2.9$

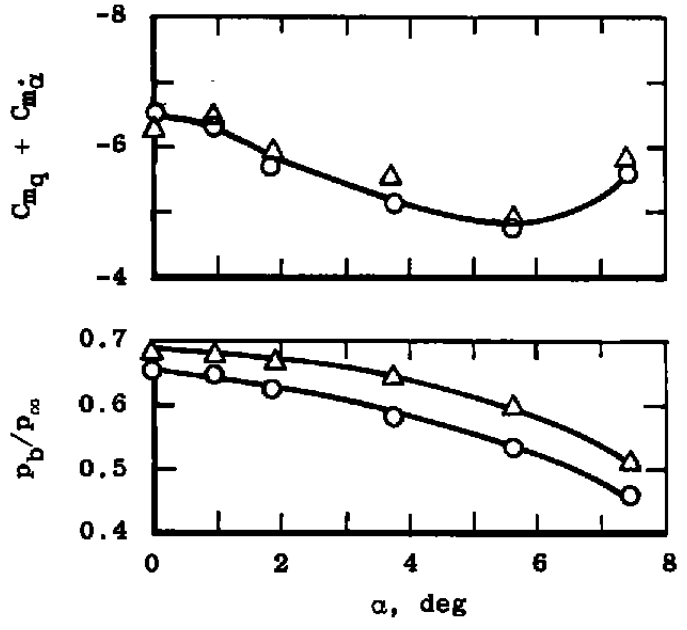

e. Plate 1, $Re_d = 4.5 \times 10^6$, $M_\infty = 3.0$

Figure 14. Concluded.

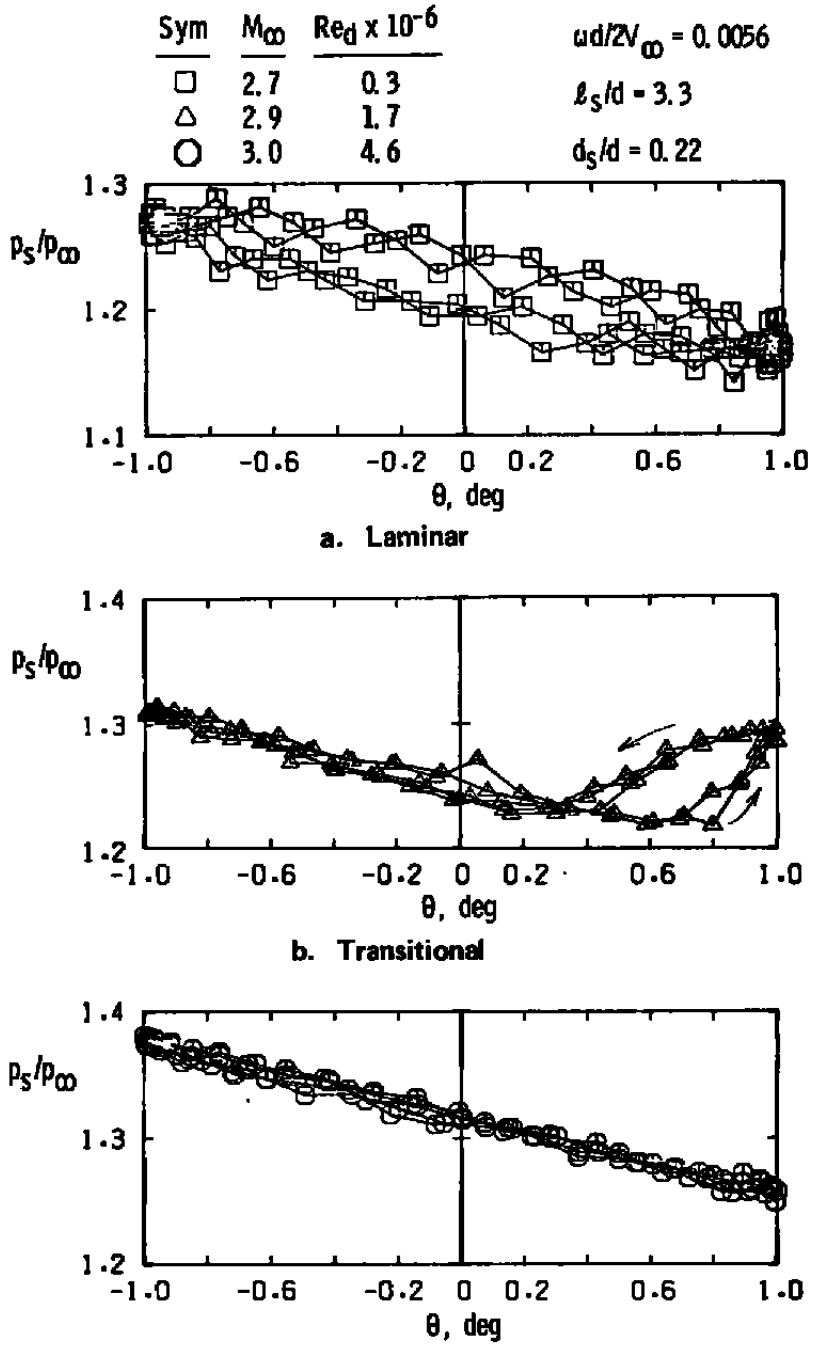

Figure 15. Surface pressure as a function of model oscillation for different boundary layers at model base, $\alpha = 0$.

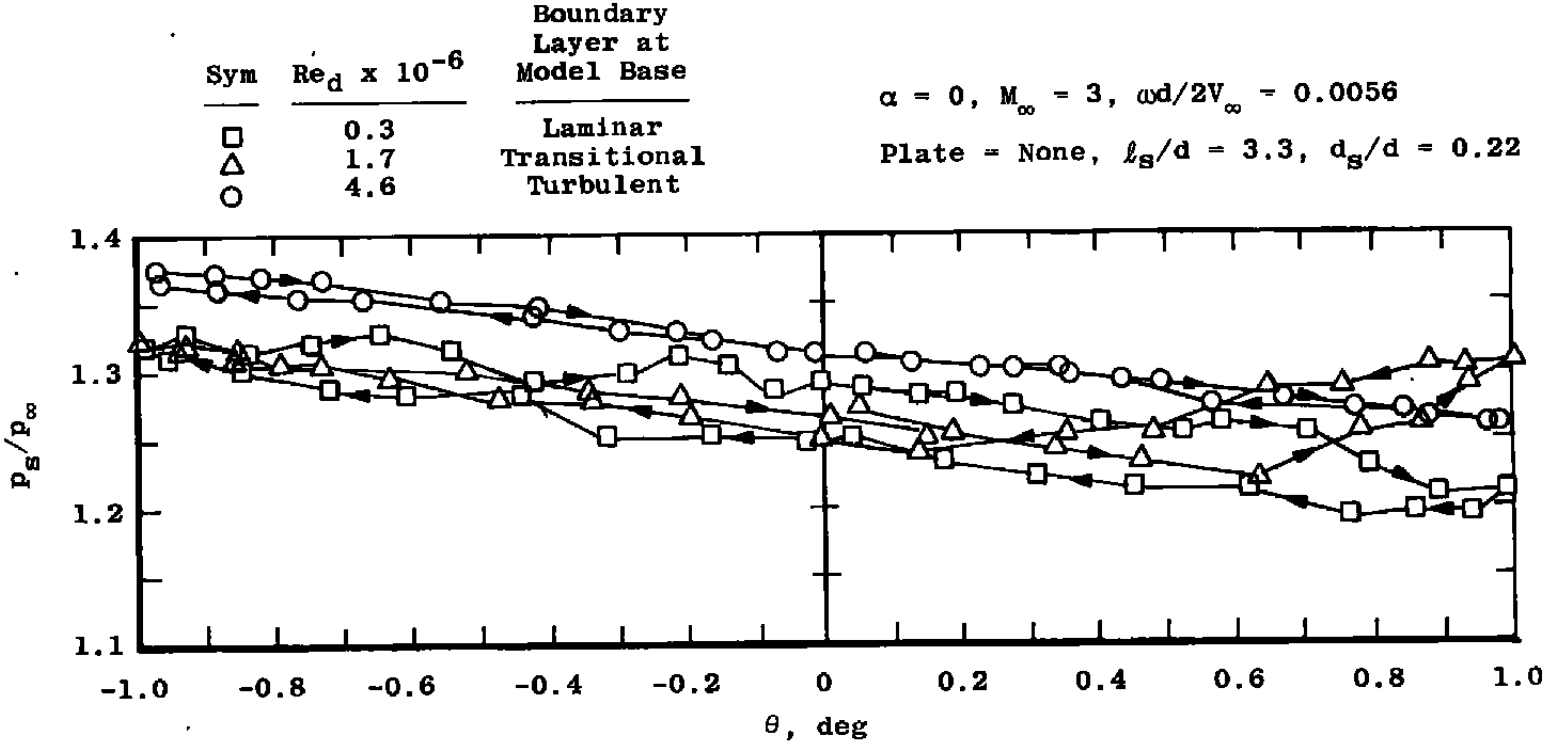

Figure 16. Surface pressure data corrected to a common Mach number of 3.

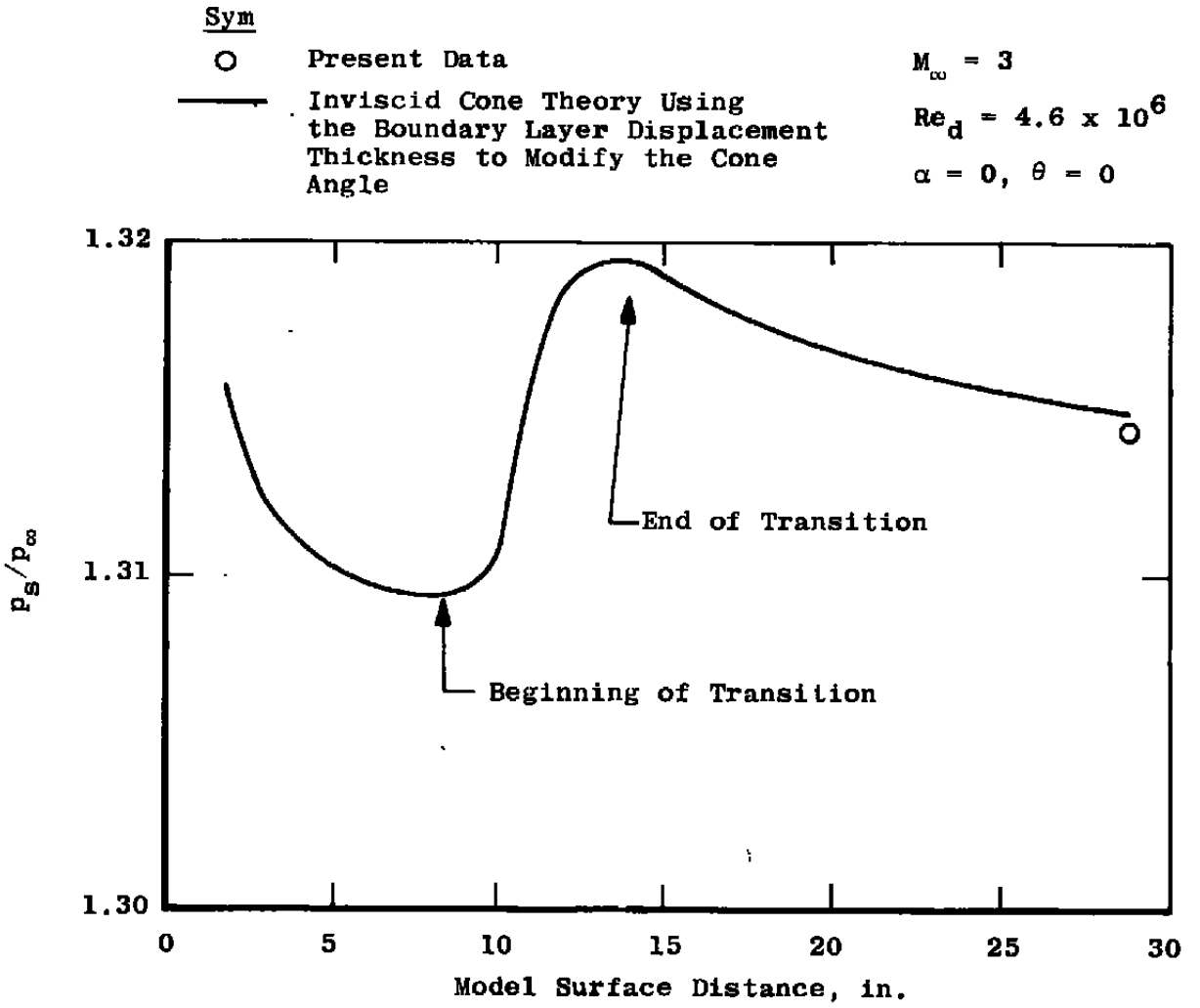

Figure 17. Theoretical pressure distribution along model surface.

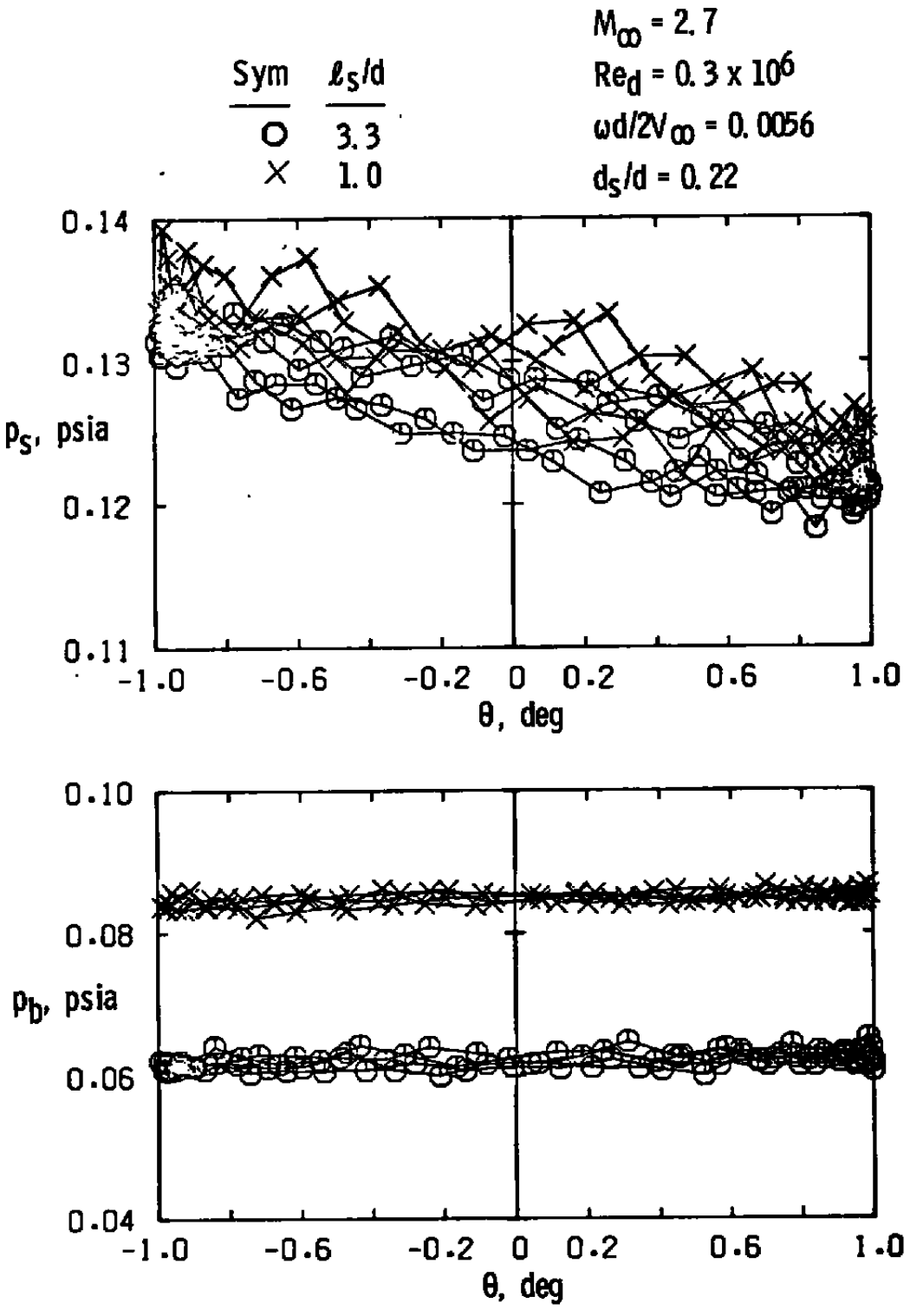

a. Laminar boundary layer at model base

Figure 18. Effect of sting length on surface and base pressure, $\alpha = 0$.

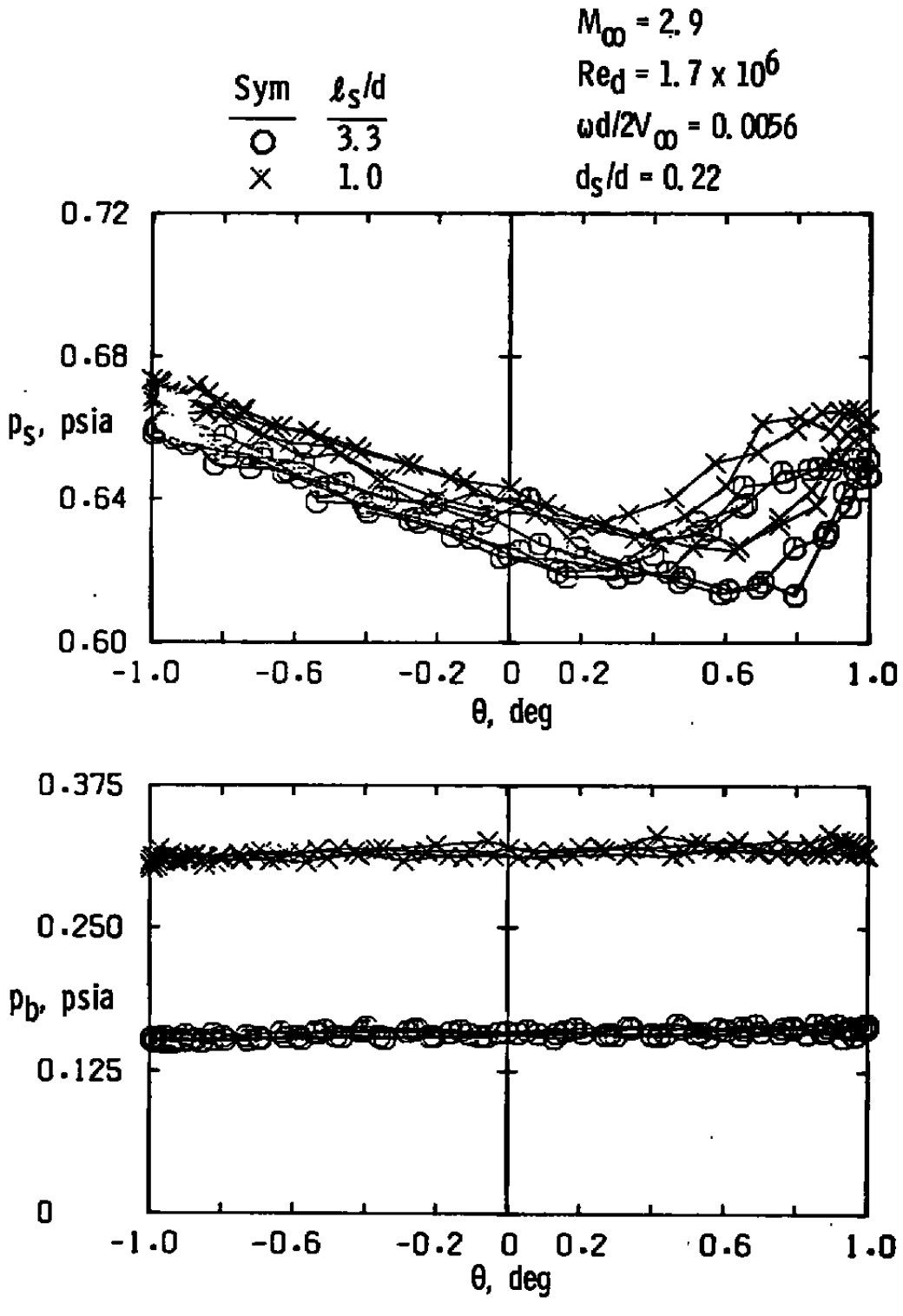

b. Transitional boundary layer at model base
Figure 18. Continued.

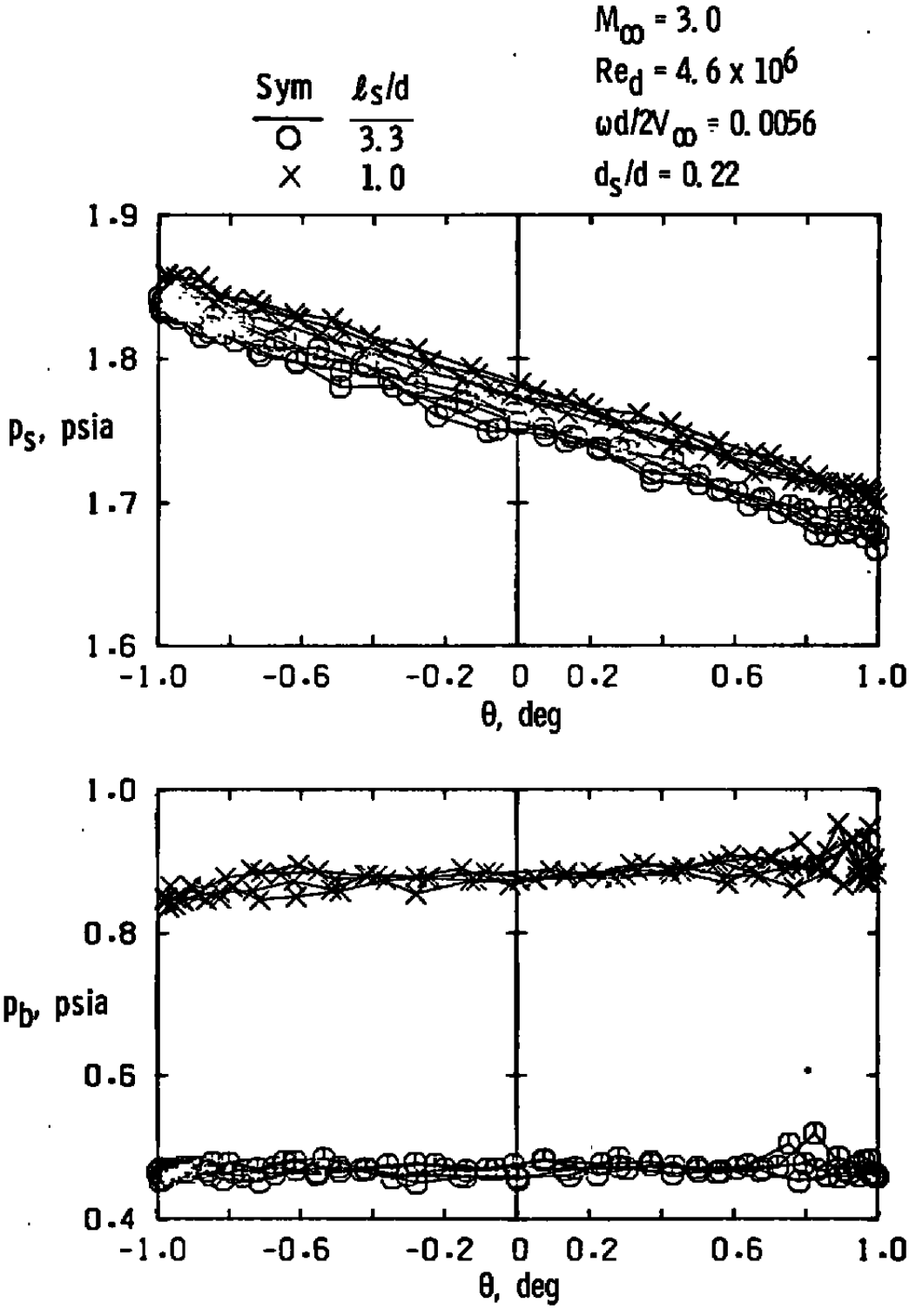

c. Turbulent boundary layer at model base
Figure 18. Concluded.

Table 1. Tunnel Conditions

Test Conditions	M_∞	$Re_d \times 10^{-6}$	p_o, psia	T_o, °R	p_∞, psi	V_∞, ft/sec	q_∞, psi
A	2.7	0.27	2.5	585	0.11	2,041	0.55
B	2.9	0.30	3.0	570	0.09	2,072	0.56
C	2.9	0.50	5.0	570	0.16	2,073	0.93
D	2.9	1.65	17.0	585	0.54	2,099	3.16
E	3.0	1.72	18.0	570	0.49	2,098	3.08
F	3.0	3.06	32.0	570	0.87	2,098	5.48
G	3.0	4.61	50.0	585	1.36	2,125	8.57

Table 2. Test Summary

$\theta = \pm 1$ deg

$\omega d/2V_\infty \times 10^3$	ℓ_s/d	Plate	Test Conditions*	α, deg
3.3	3.45	None	F	0 to 6.5
↓	3.30	↓	C, E	0
↓	↓	↓	F	0 to 6.5
↓	↓	↓	G	0 to 4.4
↓	↓	4	E	0 to 7.1
↓	↓	4	G	0 to 4.4
↓	2.50	None	C, E, F‡, G	0
↓	2.00	↓	E, F‡, G	↓
↓	1.00	↓	B, E, F‡	↓
↓	↓	↓	G	0 to 4.3
↓	↓	1	G	0 to 4.3
↓	↓	1	E	0 to 7.1
5.6	3.30	None	A+⊕, D+, G+	0 to 8.0
↓	↓	4	G	↓
↓	↓	8	D, G	↓
↓	2.50	None	G⊕	0 to 4.0
↓	2.50	↓	A, D	0
↓	2.00	↓	A, D, G	0
↓	1.00	↓	A+⊕, D+, G+	0 to 8.0
↓	1.00	1	D, G	0 to 8.0

*As Listed in Table 1

‡Data not Presented

+Oscillating Pressure Data also Obtained at $\alpha = 0$

⊕Data Presented at $\alpha = 0$ Only

NOMENCLATURE

A	Reference area (based on model base diameter (d)), 0.349 ft^2
C_A	Forebody axial-force coefficient, forebody axial force/ $q_\infty A$
C_N	Normal-force coefficient, normal force/$q_\infty A$
C_m	Pitching-moment coefficient, pitching moment/$q_\infty Ad$
C_{m_q}	Pitching-moment coefficient due to pitch velocity, $\partial(C_m)/\partial(qd/2V_\infty)$, 1/radian
C_{m_α}	Pitching-moment coefficient due to angle of attack, $\partial C_m/\partial\alpha$, $radian^{-1}$
$C_{m_{\dot\alpha}}$	Pitching-moment coefficient due to rate of change of angle of attack, $\partial(C_m)/\partial(\dot\alpha d/2V_\infty)$, 1/radian
d	Reference length (model base diameter), 0.667 ft
d_s	Effective sting diameter (at model base, see Figs. 4, 6, and 7), 1.76 in.
ℓ	Model length, in.
ℓ_{cr}	Critical sting length, in. (for $\ell_s < \ell_{cr}$, model data are affected)
ℓ_s	Effective sting length (from model base to sting flare, see Figs. 4, 6, and 7), in.
M_∞	Free-stream Mach number
p_b	Model base pressure (see Fig. 3), psia
p_o	Tunnel stilling chamber pressure, psia
p_s	Model surface pressure, psia

p_∞	Free-stream static pressure, psi
q	Pitching velocity, radian/sec
q_∞	Free-stream dynamic pressure, psi or psf
Re/ft	Free-stream Reynolds number per ft
Re_d	Free-stream Reynolds number based on reference length (d), Re_d = (Re/ft) (d)
Re_ℓ	Free-stream Reynolds number based on model length (ℓ), Re_ℓ = (Re/ft) (ℓ)
r_b	Model base radius, in.
r_n	Model nose radius, in.
T_o	Tunnel stilling chamber temperature, °R
V_∞	Free-stream velocity, ft/sec
α	Angle of attack, deg
$\dot{\alpha}$	Time rate of change of angle of attack, radian/sec
θ	Oscillation amplitude, deg
θ_c	Cone half-angle, deg
ω	Oscillation frequency, radian/sec
$\omega d/2V_\infty$	Reduced frequency parameter, radian